Deep-Sea Research I 69 (2012) 82–99

Contents lists available at SciVerse ScienceDirect

Deep-Sea Research I

journal homepage: www.elsevier.com/locate/dsri

Standing stocks and body size of deep-sea macrofauna: Predicting the baseline of 2010 *Deepwater Horizon* oil spill in the northern Gulf of Mexico

Chih-Lin Wei [a,*], Gilbert T. Rowe [b,d], Elva Escobar-Briones [c], Clifton Nunnally [d,e], Yousria Soliman [f], Nick Ellis [g]

[a] *Ocean Science Centre, Memorial University of Newfoundland, St. John's, NL, Canada A1C 5S7*
[b] *Department of Marine Biology, Texas A&M University at Galveston, Galveston, TX 77554, USA*
[c] *Universidad Nacional Autónoma de México, Instituto de Ciencias del Mar y Limnología, 04510 México D.F., México*
[d] *Department of Oceanography, Texas A&M University, College Station, TX 77843, USA*
[e] *Department of Oceanography University of Hawaii, Manoa, Honolulu, HI 96822, USA*
[f] *Biological and Environmental Sciences, Qatar University, 2713 Doha, Qatar*
[g] *CSIRO Marine and Atmospheric Research, Ecosciences Precinct, GPO Box 2583, Brisbane, QLD 4001, Australia*

ARTICLE INFO

Article history:
Received 10 April 2012
Received in revised form
9 July 2012
Accepted 17 July 2012
Available online 27 July 2012

Keywords:
Standing stock
Body size
Deep-sea
Macrofauna
Gulf of Mexico
Deepwater Horizon oil spill
Mississippi Canyon
Remote sensing
Ocean color
Primary production
Export POC flux
Random Forest modeling

ABSTRACT

A composite database encompassing 6 benthic surveys from years 1983 to 2003 was constructed to evaluate the distribution of macrofaunal biomass in the deep Gulf of Mexico (GoM) prior to the *Deepwater Horizon* oil spill. Predictive models based on optimal scaling of ocean color data and high resolution bathymetry were employed to map the benthic biomass in the vicinity of spill site because no previous sampling had been conducted at that exact location. The predicted biomass declines with water and mixed layer depth and is an increasing function of surface primary production and temporal variation of sea surface temperature. The decline of animal size with depth, however, was a function of a shift of dominant abundance from large to small taxa. At a local scale, high benthic biomass in the N GoM was associated with the enhanced productivity by the nutrient-laden Mississippi River outflows, offshore transport of the river plumes, and upwelling along the northern edge of the Loop Current. The apparent biomass enhancement at the Mississippi and De Soto Canyon and deep sediment fan was presumably related to lateral down-slope advection of organic carbon from the surrounding continental margin. Except for the Campeche Bank, the meager biomass of the Mexican margin may reflect the characteristic low-productivity Caribbean water that enters the GoM through Yucatan Strait. Benthic biomass in the N GoM was not statistically different between comprehensive surveys in the years 1983–1985 and 2000–2002. The stock assessment and biomass predictions from 669 cores at 170 locations throughout the deep GoM provide an important baseline of the sediment-dwelling fauna that may be subjected to immediate or long-term impacts from the oil spill or from climate change.

1. Introduction

1.1. Deepwater Horizon oil spill

On April 20, 2010, methane gas erupted ~1500 m below the sea surface from the Macondo well (Mississippi Canyon Block 252 or MC252), triggering explosions at the *Deepwater Horizon* (DWH) Platform. Gas, produced water, drilling mud, and crude oil gushed from the seafloor for 84 consecutive days, releasing 4.4 ± 20% million barrels of oil, causing the largest offshore oil spill in US history (Crone and Tolstoy, 2010). On the order of ~25% of oil was recovered from the wellhead or burned/skimmed at the surface. The remaining ~75% of oil evaporated, was degraded naturally through microbial oxidation, formed aggregates with suspended sediments and drilling mud and sank to the seabed or entered bays and estuaries (Lehr et al., 2010). Oil entered the marine food web (Graham et al., 2010; Hazen et al., 2010; Valentine et al., 2010) and eventually may affect the benthic community if and when the assimilated carbon reaches the seafloor (Joye and MacDonald, 2010). To prevent shoreline contamination, approximately 2.2 million gallons of chemical dispersant (COREXIT) was applied at the wellhead (0.77 M) and at the surface (1.4 M) to emulsify and thus disperse the oil within the water column (Kujawinski et al., 2011). As this strategy seemed to spare the coastline from catastrophic loss of juvenile fish cohorts after the incident (Fodrie and Heck, 2011), opinions are growing that the acute effects of the DWH oil spill will be in the deep-sea

* Corresponding author. Current address: Ocean Science Centre, Memorial University of Newfoundland, St. John's, NL, Canada A1C 5S7.
Tel.: +1 409 256 4964.
E-mail addresses: cwei@mun.ca, chihlinwei@gmail.com (C.-L. Wei).

0967-0637/$ - see front matter © 2012 Elsevier Ltd. All rights reserved.
http://dx.doi.org/10.1016/j.dsr.2012.07.008

environment (Adcroft et al., 2010; Camilli et al., 2010; Lu et al., 2012). A major concern is that the large-scale and subsea application of dispersant may alter the fate and dispersal of the spilled oil and increase the bioavailability of oil constituents to organisms in the water column and on the seafloor (Hemmer et al., 2011).

1.2. Potential effects on deep-sea macrobenthos

The biological effects of oil contamination depend on the fate of the spilled oil and the additive toxicity of individual petroleum compounds, especially the aromatic hydrocarbons that are known to have narcotic and carcinogenic toxicity (Coleman et al., 2003). The lethal and sublethal effects include individual mortality, alterations in population recruitment, growth, and reproduction, as well as changes in community structure (Coleman et al., 2003). Benthic infauna such as spionid and capitellid polychaetes and ampeliscid amphipods have been studied extensively as bio-indicators due to their resilience or sensitivity to oil contamination (Dean, 2008; Gesteira and Dauvin, 2000). For example, Montagna and Harper (1996) found that the density of non-selective deposit-feeders (polychaetes, oligochaetes and nematodes) was enhanced in the sediments near oil production platforms whereas the density of crustaceans (amphipods and harpacticoid copepods) declined due to their sensitivity to the oil toxicants. At the head of the Mississippi Canyon ($\sim$500-m depth), dense mats of tube-dwelling amphipod species ($>$12,000 individuals m^{-2}), *Ampelisca mississppiana* (Soliman and Wicksten, 2007), were discovered prior to the DWH oil spill. Their tissues showed preferential bioaccumulation of polycyclic aromatic hydrocarbons (PAHs), possibly related to drilling activities in the vicinity and anthropogenic sources from river discharge and atmospheric deposition (Soliman and Wade, 2008; Wade et al., 2008). Specimens of *A. mississippiana* appeared to tolerate moderate PAHs toxicity, but it is probably because the background concentrations were not high enough to adversely affect the biota (Wade et al., 2008). While the dissolved forms of hydrocarbons are the most bioavailable (Coleman et al., 2003), the PAHs accumulated in the tissues of marine benthos (such as amphipods) can be available to higher trophic levels through direct ingestion. The sessile macrobenthos could also be subjected to prolonged hypoxia induced by excessive microbial methane oxidation (Adcroft et al., 2010; Kessler et al., 2011). The effects could mimic the responses of macrobenthos to oxygen minimum zones (OMZs), where density and biomass reductions have been observed at the lowest oxygen concentrations (Levin, 2003). Echinoderms, crustaceans, and mollusks could be replaced by hypoxia-tolerant nematodes (Rowe, 1971) and annelids (Levin, 2003). Reduction in species richness and dominance of one or a few endemic species can also be expected in the OMZs (Levin and Sibuet, 2012). Based on previous studies in shallow water and estuaries, standing stocks of macrobenthos may decline immediately after initial spill impact (Gesteira and Dauvin, 2000; Grassle et al., 1981). The recovery of the littoral community is expected to be slower than the exposed shores, because the habitat has been contaminated by sedimentation of oil-polluted particles with no practical clean up strategies (Kingston, 2002). At $\sim$1500-m depth near the wreckage of DWH platform, low temperature (4 °C) and lack of sunlight impede natural degradation of oil in the water column or sediments; hence, the benthos could be subjected to chronic exposure to the hydrocarbons and the recovery time could be long.

1.3. Historical standing stock pattern and physical setting

The earliest quantitative macrofaunal sampling in the deep GoM began in the 70's (Pequegnat et al., 1990; Rowe and Menzel, 1971; Rowe et al., 1974). These studies suggested that the standing stocks of macrobenthos were depauperate compared to the NW Atlantic. Most of these observations can be generalized by an exponential decline of standing stocks with depth due to deteriorating quantity and quality of photosynthetic carbon that sinks to the seafloor (Rex et al., 2006; Rowe, 1983; Wei et al., 2010b). The overall level of stocks, however, varies among continental margins, depending on surface production, width of the continental shelf, latitude, and terrestrial runoff (Gage and Tyler, 1991; Rowe, 1983). Based on in-situ experiments, macrobenthos can rapidly respond to and process a pulse of fresh phytodetritus to the seabed (Sweetman and Witte, 2008; Witte et al., 2003), presumably because of their ability to quickly move to the newly settled fecal pellets, aggregates, or detritus before these resources can be utilized by small metazoan invertebrates and microbes (Rowe and Deming, 2011); hence, the macrofaunal standing stocks can be considered as a surrogate for benthic food supplies arriving on the seafloor (Johnson et al., 2007; Smith et al., 1997). In the N GoM, the surface production and the export flux of particulate organic carbon (POC) to the benthic environment were estimated to be higher in the northeast than in the northwest basin due to higher inputs of nutrients to the NE GoM (Biggs et al., 2008). Furthermore, the Mississippi Submarine Canyon in the NE GoM is an active conduit of organic matter between the productive continental shelf receiving major riverine inputs (e.g. the Mississippi River) and the sediment fan adjacent to the nutrient-poor abyssal plain at the middle of the GoM basin (Bianchi et al., 2006; Santschi and Rowe, 2008). In contrast with the prominent canyon features in the NE GoM, the continental slope of NW GoM is known for its complex physiography (Bryant et al., 1991), where numerous salt diapirs and small basins may trap and accumulate particulate organic material. In the S GoM, the Mexican margin is characterized by meager surface production in Caribbean source water that enters the Strait of Yucatan (Wiseman and Sturges, 1999). These regional differences in productivity regimes may affect the benthic food supplies and limit the distribution and standing stocks of deep-sea macrobenthos.

1.4. Census of marine life efforts and study objectives

Given the mounting challenges of climate change and anthropogenic impacts on marine ecosystems, the Census of Marine Life (CoML) was launched in 2000 to document the global baseline on marine biodiversity (McIntyre, 2010; Snelgrove, 2010). A Census-affiliated field project, the Deep Gulf of Mexico Benthos (DGoMB) program (Rowe and Kennicutt, 2008), sponsored by the Mineral Management Service (MMS), now the Bureau of Ocean Energy Management (BOEM) of US Department of Interior, began a 3-year deep-sea survey to understand the structure and function of benthic communities prior to ultra-deepwater drilling in N GoM ($>$ 1524-m depth, Richardson et al., 2008). In this analysis, regional variability of macrofaunal biomass was examined among major oceanic features in the N GoM with contrasting productivity regimes. The biomass from the DGoMB sampling was also compared with the historical data in the N GoM and new information from the S GoM. Here, the goal is to provide a baseline condition of macrofaunal stocks for future assessment of the DWH oil spill impacts. Since no previous sediment samples had been taken at the spill site (MC252), the macrofaunal biomass was reconstructed using predictive models based on bathymetry and remotely sensed ocean color images. Similar modeling has been utilized by the CoML Fresh Biomass Synthesis to predict global seafloor biomass with encouraging accuracy (Wei et al., 2010b). The complete assessment of the magnitude and effects of the DWH oil spill, however, are still under the US Natural Resources Damage Assessment (NRDA) process. The NRDA results remain largely restricted and the account provided in this study is unrelated to and independent from the NRDA process.

2. Materials and methods

2.1. Northern Gulf of Mexico (GoM) sampling

During the Deep Gulf of Mexico Benthos (DGoMB) field work (years 2000–2002, Rowe and Kennicutt, 2008; Rowe and Kennicutt, 2009), benthic macrofauna were sampled using a 0.2-m^2 version of the GOMEX box corer (Boland and Rowe, 1991). A total of 51 locations (Fig. 1, Table A1) were sampled from which the distribution of macrofauna abundance and mean size along the continental slope and abyssal plain were determined (from 213 m to 3732 m). At least 5 box cores were deployed at each location and overall 271 box cores were collected for a total sampled area of 54 m^2. Standard sample processing procedures for deep-sea benthos were used on board and in the laboratory (detailed descriptions can be found in Wei et al., 2010a). Density was estimated from specimens retained on a 300-μm sieve. Macrofauna sensu-stricto density (excluding large size meiofauna such as nematodes, harpacticoids, and ostracodes) was also estimated (Gage et al., 2002). At selected continental slope sites (C7, MT1, MT3, MT6, S36, and S42), bio-volume of individual specimens was measured using an ocular micrometer from 3 sub-cores (12.4 cm diameter) with appropriate morphometric formulae. The volume was converted to soft-body wet mass assuming a density of 1.13 mg mm^{-3} (Gerlach et al., 1985). Total biomass at each location was estimated by summation of density multiplied by the mean wet weight for each taxon (Table A2).

The Northern Gulf of Mexico Continental Slope (NGoMCS) Study (years 1983–1985, Gallaway, 1988; Pequegnat et al., 1990) used a 0.06-m^2 version of the GOMEX box corer. Animal density was estimated using the same sampling procedure (e.g. 300-μm sieve) for 45 sites based on 324 core replications from 298 to 2951-m depth (Fig. 1, Table A3). Macrofaunal body size was not measured directly during the NGoMCS; therefore, the biomass was estimated by multiplying the abundance with mean weight of major taxonomic groups from the DGoMB sampling (Table A2). Additional historical data on the Sigsbee Abyssal Plain (Rowe et al., 2003) are listed in the Supporting information (Fig. 1, Table A4). Except for a slightly smaller sieve size (250 μm), Rowe et al. (2003) used the same GOMEX box corer and sampling procedures as the DGoMB study.

2.2. Southern Gulf of Mexico (GoM) sampling

Macrofaunal data of the S GoM were provided by *Universidad Nacional Autónoma de México* (UNAM) for comparison. A total of 73 stations from 38 m to 3795-m depth were sampled from 1996 to 2003 during the *Oceanografía del Golfo de México* (OGMEX, Escobar-Briones and Soto, 1997), *Procesos Oceánicos y Mecanismos de Producción Biológica en el sur del Golfo de México* (PROMEBIO, Escobar-Briones et al., 2008a), and SIGSBEE Cruises (Arredondo, 2011; Escobar-Briones et al., 2008b; Plaza-Reséndiz, 2006). The infauna specimens were collected using a 0.2-m^2 Smith McIntyre Grab (OGMEX), 0.16-m^2 USNEL box corer (PROMEBIO), 0.25-m^2 USNEL box corer (SIGSBEE2 and SIGSBEE3), and multiple corer (SIGSBEE6). The UNAM samples were sieved with a 250-μm sieve (Fig. 1, Table A4). Preserved wet weights were measured directly on a microbalance after sorting to major taxa.

2.3. Hypothesis testing and statistical analyses

We focused on fine-scale spatial comparisons within the DGoMB study (Rowe and Kennicutt, 2008, location names in Fig. 1). A total of four null hypotheses were designed to test whether the macrofaunal biomass was different among the following geographic features in the N GoM:

(1) The active Mississippi Canyon (MT transect) and adjacent continental slope (C, WC, W, and RW transects). The RW transect includes Station AC1 and all the RW stations. The WC transect includes Stations WC5, WC12, NB2 to NB5, and BH.

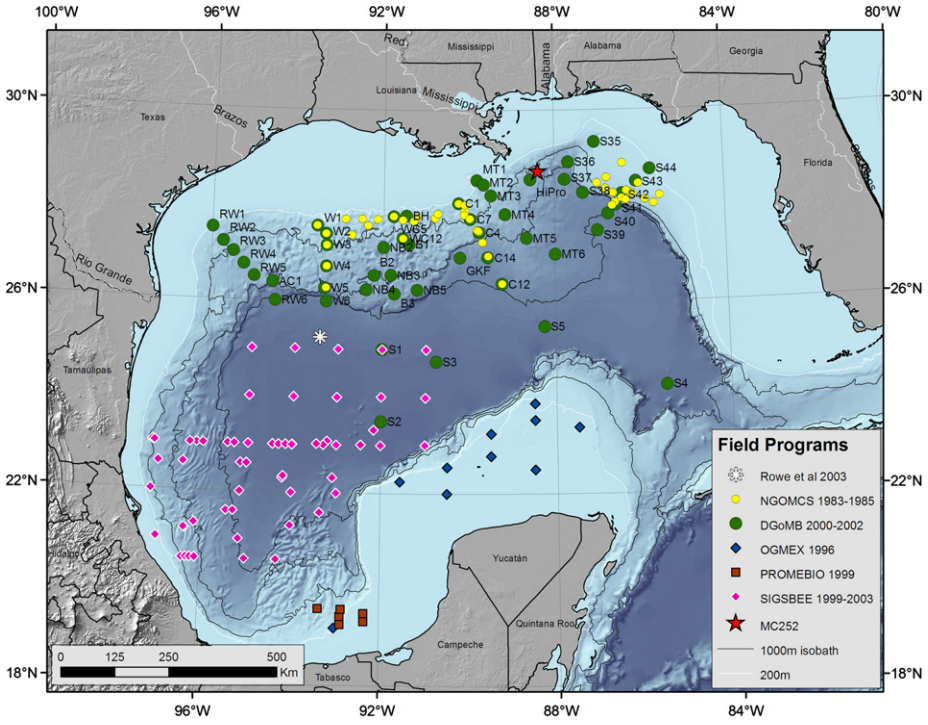

Fig. 1. Locations of quantitative deep-sea macrofauna sampling in the Gulf of Mexico. The white line indicates depth of 200 m. The black lines indicate 1000 m isobaths. The station names show the DGoMB sampling. The star symbol indicates the location of the *Deepwater Horizon* oil platform (MC252).

(2) The inactive De Soto Canyon (DS transect) and adjacent continental slope (FL transect). The DS transect includes Stations S35 to S38 and the FL transect includes Stations S44 to S39.
(3) The FL transect cutting across the steep Florida Escarpment and the RW & W transects across the relatively gradual Sigsbee Escarpment.
(4) The continental slope basins (B stations) and the adjacent non-basin slope (NB stations).

Additional null hypotheses were also employed to test whether the biomass was different between:

(5) The 2000-02 DGoMB and the earlier 1983-85 NGoMCS sampling in the N GoM.
(6) The N GoM (DGoMB+NGoMCS data) and S GoM (UNAM data) sampling.

Macrofaunal preserved wet weights were converted to organic carbon weights based on conversion factors for each taxonomic group (Rowe, 1983, Table A2) and then $\log_{10}$-transformed to approximate normality and equal variance assumption. When the parametric assumptions were not completely satisfied, the same analyses based on rank-transformed data were employed for cross-validation (Conover, 1999; Conover and Iman, 1982). We used analysis of covariance (ANCOVA) to compare the slope and elevation of regression lines (depth as functions of biomass) among transects and to remove unexplained variability associated with sampling depths (covariate). When the regression slopes were homogeneous, the elevations of regression lines were compared using Tukey's Honest Significance Difference (HSD) test (Zar, 1984). When the slopes were heterogeneous (significant interaction between treatment and covariate), Tukey's HSD test was applied to identify which pairs of transects had significantly different regression slopes (Zar, 1984). These transect pairs were compared using the Johnson–Neyman (J–N) test (Huitema, 1980) to pinpoint the specific depth ranges where the regression elevations were not significantly different. The depths outside of the non-significant ranges (based on the J–N test) and overlapped between the transect pairs (with heterogeneous regression slopes) were reported.

In selected transects (C stations, Stations W1 to W5, Stations WC5 and WC12), the DGoMB study repeated the historical NGoMCS sampling (Fig. 1). Three sites on the FL Transect, Stations S41 to S43, were also sampled in the proximity of historical NGoMCS sites (~7.1–10.5 km apart). Hence, the null hypothesis number 5 (sampling time) was also tested using randomized complete block (RCB) analysis of variance (ANOVA), with the blocking factor being the sampling sites along the selected transect.

2.4. Random forest modeling

Random Forest (RF) models (Breiman, 2001) were constructed to fit $\log_{10}$ macrofaunal biomass on multiple environmental predictors. In the RF, 2/3 of the biomass observations (from the core replications) were subjected to successive binary partitions. At each split point, an optimal split value (S) was chosen from a random subset of environmental predictors (from 1/3 of all the variables) to divide the biomass data into left ($<$S) and right groups ($\geq$S). A selection criterion was making the stock data within each group as homogeneous as possible, with continued partitioning until no further division can be made. This resample process (with replacement) was repeated 1000 times and the tree-like structures were collected. Similar to a regression model with a mathematical equation, predictions were made by passing new environmental data through the individual trees following the decision rules. The terminal answers from each tree were then averaged as the final predictions.

For each decision tree, the roughly 1/3 of the unused biomass data (out-of-bag or OOB data) can independently verify the model goodness of fit (R^2) against the predictions from corresponding predictors. The importance of a predictor can be evaluated by independently permuting its values within the OOB data. This is to mimic the absence of that variable; hence, the increase of mean square error (or deterioration of the R^2) after the permutation quantifies the variable's importance. Based on this concept, we employed an improved "conditional permutation" algorithm (Ellis et al., 2012; Strobl et al., 2008), in which the predictor values were permuted within partitions of the values for the correlated predictors ($\rho > 0.5$, Pearson's correlation). This new algorithm corrects the assumption that the predictors are independent of each other (independent permutation) and also reduces the bias of spurious correlations.

After identifying the most influential predictors, we used a partial dependence plot (Friedman, 2001) to visualize their effects on the predicted biomass, or how the RF model responds to these variables. For example, to evaluate the effect of 1000-m depth on biomass model, all the actual depth observations (669 replications in our case) were replaced with 1000 and then the new synthetic data matrix (along with ocean color observations) was passed through the existing model to make the prediction. The new average value from the 669 predictions is then the partial dependence at depth of 1000 m, measuring the depth effect on model response while accounting for the average effect of other predictors. This averaging procedure was repeated across the depth gradient to evaluate the model response as a function of depth. The same procedure was conducted for other influential predictors.

2.5. Environmental predictors and scaling simulations

Predictors used monthly ocean color images from October 1997 to December 2007 based on the Sea Viewing Wide Field-of-view Sensor (SeaWiFS r2010) and Advanced Very High Resolution Radiometer (AVHRR) and from January 2008 to December 2010 based on the Moderate Resolution Imaging Spectroradiometer (MODIS r2010, Table 1). The switch from the SeaWiFS to MODIS data is necessary because the SeaWiFS was decommissioned in 2010 and only had sketchy temporal coverage for the latter period. The images of three net primary production (NPP) models and seven parameters for building these NPP models were obtained from the Ocean Productivity web page to represent the complete state of surface productivity during the 13-plus year period (full predictor attribution in Table 1). In addition, water depths measured during original benthic surveys were also included as a predictor (Table A1, A3, and A4). The full coverage of the GoM bathymetry was obtained from the NOAA Geophysical Data Center.

Prior to extracting the ocean color data, images of sea surface temperature (data prior to January 2008) and mixed layer depth were re-gridded to 5 arc-min grids (by re-defining the grid spaces) to match the resolution of other images (Table 1). The sampling year of earlier studies (before year 2000, Table A3 and A4) was set to the year of 2000. Coordinates of sediment cores were matched to the satellite images at the time of the sampling (based on year and month). This direct matching approach, however, is also subject to bias, because macrofauna stocks are not necessarily concurrent with surface primary production (Johnson et al., 2007). The time for detrital materials to sink to the seafloor (Asper et al., 1992) and for the macrobenthos to respond to changes of food supply (Sweetman and Witte, 2008;

Table 1
Environmental data for Random Forest analysis. The unit of image resolution is arc-minutes. Abbrev denotes the variable abbreviation.

Image resolution		Abbrev	Variable	Unit
Monthly Mean and S.D. of ocean colors (www.science.oregonstate.edu/ocean.productivity)				
SeaWiFS	MODIS			
1997–2007	2008–2010			
5	5	vgpm	Standard vertical general production model	mg C m^{-2} d^{-1}
5	5	eppley	Eppley vertical general production model	mg C m^{-2} d^{-1}
5	5	cbpm	Carbon based production model	mg C m^{-2} d^{-1}
5	5	chl	Chlorophyll a concentration	mg m^{-3}
5.3	5	sst	Sea surface temperature	°C
5	5	par	Photosynthetic radiation	einstein m^{-2} d^{-1}
5	5	bbp	Particulate backscatter	m^{-1}
10	10	mld	Mixed layer depth	m
5	5	growth	Phytoplankton growth rate	divisions d^{-1}
5	5	carbon	Carbon concentration	mg m^{-3}
ETOPO1 Global Relief Model (www.ngdc.noaa.gov/mgg/global)				
1	1	depth	Water depth	m

Witte et al., 2003), as well as complex hydrographic regimes (Jochens and DiMarco, 2008), may complicate the scaling of the satellite data. More likely, the macrobenthos is affected by the overlying conditions of a large area and through a substantial time period before the sampling. To cope with this scaling issue, the following extraction scenarios were tested:

(1) The time lags between satellite images and benthic sampling (from 0 to 24 months prior to the time of sampling).
(2) The catchment radius circling the sample location (grid cells within 0 to 120 arc-min radius in 5 arc-min increments).
(3) The accumulating time windows (starting from 0 to 5 months prior to the lag month).

For example, a typical extraction of one ocean color parameter for one sample (or sediment core) includes the following steps:

1) Selecting multiple images from a desired accumulating time window (prior to the sampling).
2) Calculating mean cell values within a desired catchment area for all selected images.
3) Averaging those mean values and calculating standard deviation (SD) over the time period.

The final mean and SD representing the overall level and variation within the time window together with water depth (a total of 21 variables, Table 1) were used as predictors to run the RF analysis. The biomass predictions were made based on the best fitting RF models to the empirical data (highest R^2). We used an average index to assemble the outputs from multiple top models. The model uncertainty was then evaluated by the coefficients of variation (CV, mean/SD × 100%). Because most of the benthic sampling was conducted in early summer (32.9% in May and 40.7% in June), we set the prediction target to the month of June. For making predictions, new ocean color data were reprocessed based on the known temporal and spatial scaling and then combined with bathymetry before being passed to the selected top models.

The utility of reduced models (based on subsets of environmental data) was also examined. This was done by monitoring the RF performance (R^2) while step-wise eliminating the least important or step-wise adding the most important predictors. Specifically, the two approaches started from the same rank of predictor importance (full model, 21 variables). For the step-wise elimination, the predictor importance was re-examined (by running separate RF) at each step for the predictors within the reduced model. The least important predictor was then eliminated in the next step. For the step-wise inclusion, the re-examination at each step was done for the predictors not in the reduced model. The most important predictor was then removed from the next re-examination step and added to the reduced models.

Statistical analyses used R computing environment (R Development Core Team, 2011) with R packages "random Forest" (Liaw and Wiener, 2002), "extendedForest" (Ellis et al., 2012; Smith et al., 2011), and "lattice" (Sarkar, 2008). Geostatistical analyses and GIS mapping used ESRI® ArcMapTM 9.2 and R package "sp" (Bivand et al., 2008).

3. Results

3.1. Standing stocks and average size estimates in DGoMB sampling

A total of 147,270 specimens were collected and sorted into 39 macrofaunal taxa during the DGoMB study. Nematodes had the highest total abundance (30.3%) followed by polychaetes (26.2%), amphipods (13.8%), and harpacticoids (6.3%) (Fig. 2a, Table A5). The total density showed a significantly negative log-linear relationship with depth (Fig. 3a, $F_{1,49}=63.38$, $P<0.001$). The head of Mississippi Canyon (Station MT1, Fig. 1) had the highest density (Table 2, 21,801 ± 7,659 m^{-2}, $n=10$). The second highest density (~11,000 m^{-2}) occurred in the upper Desoto Canyon (Stations S35 and S36). The next level of animal density (~7000–9,000 m^{-2}) was found in the upper Mississippi Canyon (Stations MT2 and MT3) and upper slope (Stations RW1, W1, and S43). Surprisingly, the deepest site on the Mississippi Sediment Fan (Station S5 at 3314-m depth) had one of the highest animal densities (7075 ± 217 m^{-2}, $n=2$). All other abyssal sites at similar depths (Stations S1 to S4 at 3409 to 3732-m depth) only had ~800–1600 individuals m^{-2}, suggesting a 4- to 8-fold enrichment of animal density at Station S5.

When the meiofaunal taxa (harpacticoids, nematodes, and ostracodes) were removed (macrofauna sensu-stricto), the animal density appeared to decline more rapidly with depth and the linear model fit was improved (Fig. 3b, $F_{1,\ 49}=140.4$, $P<0.001$). The hierarchy of animal density among sites showed an apparent shift. The head of the Mississippi Canyon (Station MT1, Fig. 1) still had the greatest density (Table 2, 21,633 ± 7,903 m^{-2}, $n=10$). The second highest density was only ~6000 m^{-2} at the upper Mississippi Canyon (Station MT2) and the shelf break of the far-west slope (Station RW1). The next level of 5000 or so individuals m^{-2} occurred at the head of Desoto Canyon (Station S35) or the shelf break of the Texas (Station W1) and Florida Slope (Station S44). Despite its mid-slope depth (1572 m), the Station

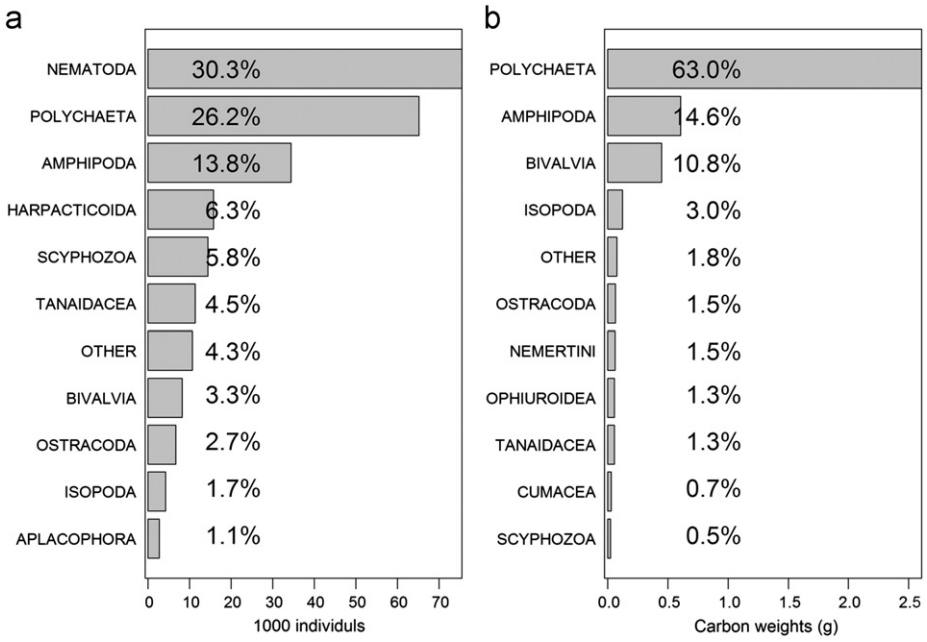

Fig. 2. Total macrofauna abundance and organic carbon biomass collected during the DGoMB study. Bar chart shows the top 10 macrofaunal taxa with highest (a) abundance and (b) organic carbon weights. The 11th to 39th most abundant taxa were combined as category "OTHER". Following the bar chart is relative abundance (a) or biomass (b) for each taxon (%).

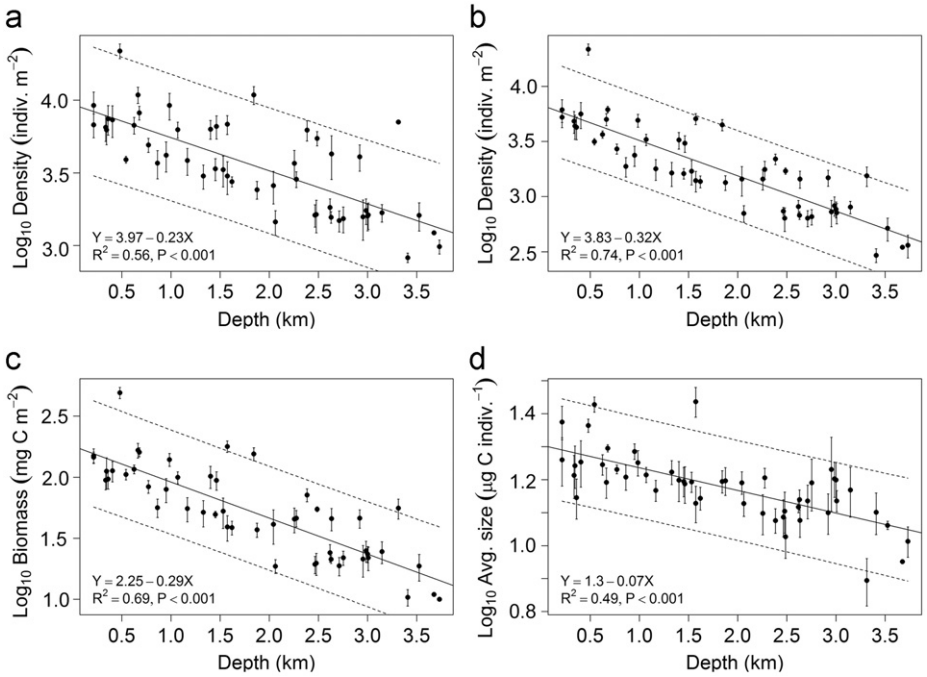

Fig. 3. Log_{10}-transformed (a) total density, (b) macrofauna sensu-stricto density, (c) organic carbon weight, and (d) average body size as functions of water depth for DGoMB sampling. Linear regressions (solid line) with 95% confidence interval (between dashed lines) were conducted on the station averages from core replications. The standard error is shown as an error bar.

HiPro had a surprisingly high sensu-stricto density ($5076 \pm 1{,}279$ m^{-2}, $n=5$) southeast of the mouth of the Mississippi River. The sensu-stricto density on the deep Mississippi Sediment Fan (S5) dropped dramatically to only $1545 \pm 438\ m^{-2}$ ($n=2$); nonetheless, it was still 3–5 times more abundant than the sensu-stricto density at Station S1 to S4 (294 to 516 m^{-2}) on the abyssal plain.

Preserved wet weights and organic carbon weights were estimated by multiplying density (Table A4) by the mean weight of each taxon (Table A2). Polychaetes contributed more than half (63.0%) of the organic carbon biomass, followed by amphipods (14.6%), bivalves (10.8%), and isopods (3.0%) (Fig. 2b, Table A6). The carbon biomass-depth trend (Fig. 3c) was similar to the trend for the sensu-stricto density against depth (Fig. 3b). The Mississippi Canyon head (Table 2, Station MT1, 492.1 ± 159.88 mg C m^{-2}, $n=10$) still had the highest biomass; however, the vicinity of Mississippi River mouth (Station HiPro, 178.8 ± 43.02 mg C m^{-2}, $n=5$) and the upper De Soto Canyon (Station S35, 166.2 ± 51.25 mg C m^{-2}, $n=5$; Station S36,

Table 2
Macrofaunal standing stocks and average size for DGoMB sampling. n=size of sample, D=density (individual m^{-2}), Dx=macrofauna sensu-stricto density (excluding nematodes, harpacticoids, ostracodes), B=preserved wet weight. (mg m^{-2}), BC=organic carbon weight. (mg C m^{-2}), W=average size (mg individual^{-1}), WC=average size (mg C individual^{-1}).

Station	n	D	S.D.	Dx	S.D.	B	S.D.	BC	S.D.	W	WC
Far West (RW) transect											
RW1	5	9202	4893	6137	3211	3257.1	728.79	145.7	32.73	0.41	0.018
RW2	5	4183	2196	2370	1087	1807.9	773.01	79.6	39.56	0.45	0.019
RW3	5	3011	1270	1641	906	1116.6	625.22	51.7	27.98	0.36	0.017
RW4	5	3009	1708	1399	660	935.2	526.50	39.1	20.60	0.32	0.013
RW5	5	2754	488	1372	378	900.8	276.63	38.6	11.13	0.32	0.014
RW6	5	1624	752	715	335	513.9	242.83	21.9	10.58	0.32	0.014
West (W) transect											
W1	5	7332	4030	5626	3334	2504.7	1022.14	112.9	47.43	0.40	0.018
W2	4	6729	1739	3662	542	2600.4	424.87	116.1	19.08	0.40	0.018
W3	5	3690	1810	1883	841	1345.3	525.30	56.3	21.59	0.38	0.016
W4	5	3377	1296	1621	400	1123.3	193.34	49.6	6.63	0.35	0.016
W5	5	1533	688	659	233	496.2	169.37	21.9	6.47	0.35	0.016
W6	5	1682	518	804	233	580.7	225.20	24.5	11.14	0.35	0.015
AC1	5	1638	924	637	344	451.0	217.16	19.7	8.98	0.29	0.013
West Central (WC) transect											
WC5	5	6248	2946	4382	2435	2419.3	1456.01	112.2	71.83	0.38	0.017
WC12	5	3843	1802	1787	856	1281.6	608.96	55.4	27.89	0.34	0.015
NB2	5	3323	1779	1700	946	1202.7	702.13	52.7	33.04	0.36	0.016
NB3	5	2420	755	1342	454	846.8	254.00	37.1	11.12	0.36	0.016
NB4	5	2582	1452	1443	966	963.2	625.75	41.1	28.78	0.37	0.016
NB5	5	1454	625	706	275	441.5	150.02	18.7	5.35	0.31	0.013
BH	5	3899	477	3143	465	2349.1	430.17	105.3	23.09	0.60	0.027
Basin (B) transect											
B1	5	3681	1866	1446	664	1040.4	519.53	45.3	23.16	0.29	0.013
B2	5	1566	321	676	125	504.4	70.76	21.2	3.44	0.33	0.014
B3	5	1827	599	814	246	608.1	224.56	24.1	8.71	0.33	0.013
Central (C) transect											
C1	5	6504	2925	4829	2419	2079.9	766.10	94.7	35.63	0.36	0.016
C7	10	6272	2485	3293	1230	2245.7	772.69	99.6	35.64	0.37	0.016
C4	5	6599	2669	3045	1167	2161.5	755.53	94.4	36.00	0.35	0.015
C14	5	5467	1358	1709	255	1275.8	82.92	54.8	5.47	0.25	0.011
C12	5	4079	1865	1485	550	1091.2	415.28	46.1	17.72	0.30	0.013
Mississippi Canyon (MT) transect											
MT1	10	21801	7956	21663	7903	10625.0	3453.72	492.1	159.88	0.50	0.023
MT2	4	8194	1777	6172	828	3643.2	618.64	160.4	26.98	0.45	0.020
MT3	10	9219	6047	4924	2087	3212.2	1239.16	139.5	53.23	0.41	0.018
MT4	5	6317	2070	3262	1252	2228.7	956.84	101.8	46.34	0.35	0.016
MT5	5	2859	783	1763	736	1055.5	358.20	46.2	15.98	0.37	0.016
MT6	9	1485	731	638	315	430.3	208.44	18.8	9.72	0.32	0.014
De Soto Canyon (DS) transct											
S35	5	10887	3103	5019	1404	3739.1	1033.66	166.2	51.25	0.35	0.016
S36	12	10859	5302	4481	1808	3488.5	1317.49	155.3	64.73	0.36	0.016
S37	5	6231	2232	2192	532	1611.3	400.43	71.5	19.33	0.27	0.012
S38	5	4268	3184	1445	566	1014.4	473.56	45.8	21.22	0.26	0.012
Florida (FL) transect											
S44	5	6776	2815	5262	2337	3141.2	901.75	150.0	46.26	0.50	0.024
S43	5	7456	3834	4265	2198	2412.0	904.70	96.6	37.41	0.35	0.014
S42	9	4917	1628	2709	858	1893.8	625.08	83.7	29.80	0.39	0.017
S40	4	1572	968	729	392	504.5	268.70	21.4	12.40	0.43	0.017
S41	8	1744	986	828	461	563.9	309.43	24.9	13.89	0.36	0.016
S39	5	1595	744	769	284	533.9	186.09	23.5	7.95	0.36	0.016
Sigsbee Abyssal Plain											
S5	2	7075	217	1545	438	1384.8	343.26	55.7	14.61	0.20	0.008
S4	4	825	124	294	84	248.0	82.15	10.4	3.18	0.30	0.013
S1	2	1612	500	516	173	414.2	140.03	18.7	6.52	0.26	0.012
S3	1	1223	N.A.	348	N.A.	260.2	N.A.	10.9	N.A.	0.21	0.009
S2	2	983	152	362	119	235.0	20.16	10.0	0.05	0.24	0.010
Other											
HiPro	5	6826	2257	5076	1279	3949.4	919.31	178.8	43.02	0.60	0.027
GKF	5	1622	634	737	132	485.5	186.87	19.3	7.01	0.30	0.012

155.3 ± 64.73 mg C m^{-2}, $n=12$) joined the upper Mississippi Canyon (Station MT2, 160.4 ± 26.98 mg C m^{-2}, $n=4$) to have the second highest biomass (Fig. 3c). The biomass of the deep Mississippi Sediment Fan (Table 2, Station S5, 55.7 ± 14.61 mg C m^{-2}, $n=2$) was still 3 to 6 times higher than the other abyssal plain areas (Stations S1 to S4, 10 to 18.7 mg C m^{-2}).

The average animal size (organic carbon weight divided by density) also declined with depth (Fig. 3d, $F_{1,\ 49}=46.81$,

$P<0.001$). Station BH (Bush Hill), a methane-seep site and Station HiPro, adjacent to the Mississippi River mouth, had the largest average animal size (Table 2, 27 μg C individual^{-1}). The relative abundance of nematodes, harpacticoids, and ostracodes (> 300 μm) increased from 0.6% at the head of the Mississppi Canyon (Station MT1) to about 78.2% on the deep Mississippi Sediment Fan (Station S5), with an increase of about 10% every kilometer of depth (Fig. 4, $F_{1,49}=61.94$, $P<0.001$). This suggests that the decreasing average size with depth was associated with increasing numbers of nematodes, harpacticoids, and ostracodes at depths. However, in relatively deep water (1572 m), Station HiPro only had about half (23.6%) as much of these taxa as other sites of similar depths (~50%, Fig. 4). The organic carbon biomass had higher correlation with the sensu-stricto density (Pearson's correlation, $\rho=0.98$, $t=84.5$, df=269, $P<0.001$) than with the overall density ($\rho=0.94$, $t=47.1$, df=269, $P<0.001$), suggesting that the carbon biomass was affected less by macrofauna sensu-stricto because the nematodes, harpacticoids, and ostracodes comprised only ~1.8% of the total biomass.

3.2. Hypothesis testing

During DGoMB sampling, organic carbon biomass declined significantly (log-linear) with depth on all 7 transects (Table 3a). The regression slopes, however, differed significantly among transects (Table 3b, ANCOVA, slope, $F_{6,\ 221}=15.01$, $P<0.001$) with the slopes of MT (Mississippi Canyon) and C Transect (central slope) being significantly different (higher and lower respectively) from the rest of the transects (Table 3c, Tukey's HSD test, $P<0.05$). The MT Transect (Fig. 5) had the most rapid decline in biomass with depth (slope = −0.57), while the C Transect had the slowest decline (slope = −0.14). Transect MT (down the axis of the Mississippi Canyon) had significantly higher biomass than RW (far-west slope), W (west slope), WC (west central slope), and FL Transect (Florida slope) between depths of 0.5 and 2.0 km (Table 3c, J-N test, $P<0.05$). The rapid decline along the MT Transect intersected with the slow decline of the C Transect (Fig. 5); hence, the biomass was significantly higher on the MT than on the C Transect between 0.5 and 1.6-km depths but was significantly lower between 1.7 and 2.7-km depths (J-N test, $P<0.05$).

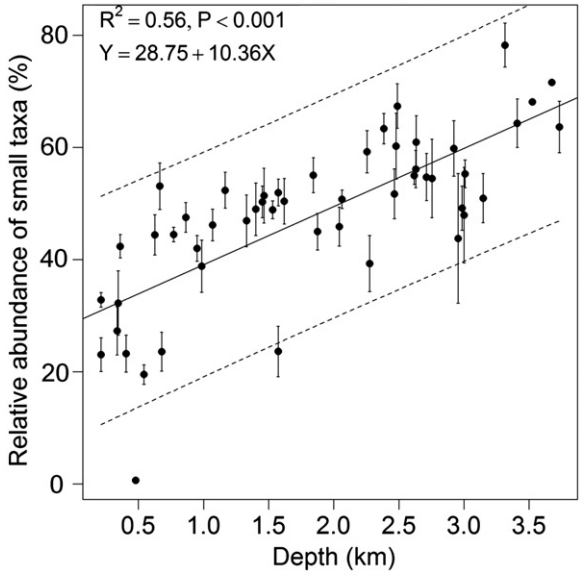

Fig. 4. Relative abundance of nematodes, harpacticoids, and ostracodes in box core samples as a function of water depth (km) during DGoMB sampling. Linear regression (solid line) with 95% confidence interval (between dashed lines) were conducted on the station averages from core replications. The standard error is shown as an error bar.

Table 3
Linear regressions and ANCOVAs for organic carbon biomass against depth during DGoMB sampling. (a) Regression statistics for each transect. The dependent variable is $\log_{10}$ biomass (mg C m^{-2}). The independent variable is depth (km). (b) ANCOVA on biomass among 7 transects. (c) Transect pairs with heterogeneous slopes (based on Tukey HSD multiple comparisons, $P<0.05$) and the depth ranges where the biomass were significantly different (Johnson–Neyman test, $P<0.05$). Inequality sign shows the direction of the difference between transects. (d) ANCOVA on biomass among transects with homogeneous slopes. (e) Tukey HSD multiple comparisons on regression elevations between transects with homogeneous slopes.

(a)	Transect	Slope	Intercept	Df1	Df2	R^2	F	P
	RW	−0.33	2.14	1	33	0.68	71.7	****
	W	−0.26	2.08	1	27	0.72	70.3	****
	WC	−0.35	2.14	1	33	0.50	32.8	****
	C	−0.14	2.08	1	28	0.36	16.0	****
	MT	−0.57	2.79	1	41	0.84	214.6	****
	DS	−0.28	2.52	1	25	0.40	16.8	****
	FL	−0.27	2.12	1	34	0.74	94.5	***
(b)	ANCOVA	Df1	Df2	SS	MS	F	P	
	Slope	6	221	3.0	0.5	11.9	****	
	Elevation	6	221	6.4	1.1	24.9	****	
(c)	Transects		Depths	P	Transects		Depths	P
	MT >	RW	0.5–2.3	**	MT <	C	1.7–2.7	**
		W	0.5–2.0	**		DS	0.8–2.6	**
		WC	0.5–2.3	**		FL	2.6–2.7	**
		C	0.5–1.6	**	C >	RW	0.7–2.9	**
		FL	0.5–2.0	**		WC	0.7–2.0	**
(d)	ANCOVA	Df1	Df2	SS	MS	F	P	
	Slope	4	152	0.2	0.0	0.9	n.s.	
	Elevation	4	152	4.4	1.1	25.0	****	
(e)	Transects		DF1	DF2	Q	P		
	DS >	RW	4	152	12.1	****		
		W	4	152	10.4	****		
		WC	4	152	11.0	****		
		FL	4	152	9.9	****		

Significance codes: n.s.: $P\geq 0.1$.
*$P<0.1$.
** $P<0.05$.
*** $P<0.01$.
**** $P<0.001$.

The steep slope of the MT Transect was associated with extremely high biomass at the Mississippi Canyon head (MT1, 492.1 ± 159.88 mg C m^{-2}, $n=10$, Table 2). At a depth of 2712 m (Station MT6), MT transect converged with the RW, W, WC, and FL Transects (Fig. 5) to 18.8 ± 9.72 mg C m^{-2} ($n=9$). The biomass of MT Transect declined so sharply with depth that it was significantly less than DS Transect (De Soto Canyon) between depths of 0.8 and 2.6 km and significantly less than FL Transect between 2.6 and 2.7 km (Table 3c, J-N test, $P<0.05$). Despite the increasing water depth, the C Transect maintained a relatively high level of biomass, being significantly higher than RW and WC Transect from 0.7 to 2.9 and to 2-km depth, respectively (J-N test, $P<0.05$).

Regression slopes of the RW, W, WC, DS, and FL Transect were not significantly different (Table 3d, ANCOVA, slope, $F_{4,\ 152}=0.9$, $P=0.48$); nonetheless, the elevations were significantly different (elevation, $F_{4,\ 152}=25$, $P<0.001$). Only the DS Transect (Fig. 5) had significantly greater regression elevation (Table 3e, Tukey's HSD test, $P<0.001$) than the other 4 slope transects (RW, W, WC, and FL).

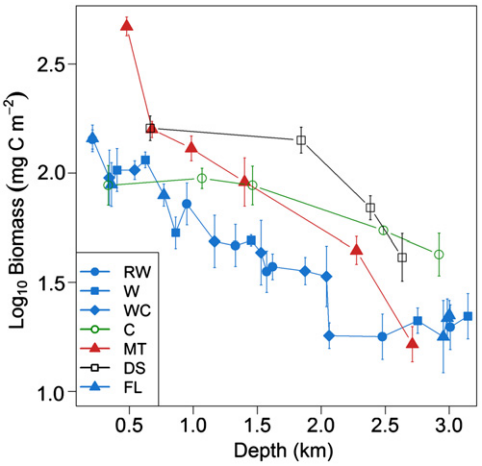

Fig. 5. Log_{10}-transformed organic carbon biomass against depth for each transect during DGoMB sampling. "MT" indicates the Mississippi Canyon transect (MT stations); "DS" indicates the De Soto Canyon transect (Station S35 to S38); "C" indicates the central slope transect (C stations); "RW" indicates far-west transect (RW stations & AC1); "W" indicates west slope transect (W stations); "WC" indicates west central slope transect (BH and WC & NB stations); "FL" indicates Florida slope transect (Station S39 to S44). Detailed locations of sites can be found in Fig. 1. Test statistics of linear regression for each transect can be found in Table 3a.

Table 4
Linear regressions and ANCOVAs for organic carbon biomass against depth among studies. (a) Regression statistics for basins (B), non-basins (NB), NGoMCS, DGoMB, N GoM (NGoMCS+DGoMB), and S GoM. The dependent variable is log_{10} biomass (mg C m^{-2}). The independent variable is depth (km). (b) ANCOVA on biomass between basin and non-basin sampling, between historical (NGoMCS) and current (DGoMB) sampling in the northern GoM, and between northern and southern half of the GoM basin.

(a)	Transect	Slope	Intercept	Df1	Df2	R^2	F	P
	B	−0.71	3.20	1	13	0.33	6.5	***
	NB	−0.49	2.42	1	18	0.16	3.5	*
	NGoMCS	−0.26	2.18	1	43	0.67	87.5	****
	DGoMB	−0.29	2.25	1	49	0.69	109.8	****
	N. GoM	−0.28	2.21	1	94	0.72	242.7	****
	S. GoM	−0.31	1.73	1	69	0.56	89.1	****
(b)	ANCOVA		Df1	Df2	SS	MS	F	P
	Basin vs Non-basin (H04)							
	Slope		1	31	0.01	0.01	0.3	n.s.
	Elevation		1	31	0.2	0.2	3.9	*
	NGoMCS vs. DGoMB (H05)							
	Slope		1	92	0.02	0.02	0.5	n.s.
	Elevation		1	92	0.02	0.02	0.6	n.s.
	N. GoM vs. S. GoM (H06)							
	Slope		1	163	0.06	0.06	0.8	n.s.
	Elevation		1	163	9.6	9.6	136.8	****

Significance codes: n.s.: $P \geq 0.1$.
**$P < 0.05$.
* $P < 0.1$.
*** $P < 0.01$.
**** $P < 0.001$.

Organic carbon biomass within small slope basins (B stations) declined log-linearly with depth (Table 4a, $F_{1,13}=6.5$, $P=0.02$), while the adjacent non-basin sites (NB stations) only showed a marginal biomass-depth relationship ($F_{1,18}=3.5$, $P=0.08$). The regression slopes were not significantly different (Table 4b, ANCOVA, slope, $F_{1,31}=0.3$, $P=0.6$) and the basin biomass was only marginally higher than the non-basin biomass (elevation, $F_{1,31}=3.9$, $P=0.06$).

Historical NGoMCS sampling showed a similar log-linear biomass-depth relationship (solid line, Fig. 6) with the current DGoMB sampling. Neither the regression slopes nor the regression elevations was significantly different between the two studies (Table 4b, ANCOVA, slope, $F_{1,92}=0.5$, $P=0.48$; elevation, $F_{1,92}=0.6$, $P=0.44$). Among transects being revisited, only the 3 sites on FL Transect (S41, S42, and S43) had significantly higher biomass for the NGoMCS than for the DGoMB study (Table 5, ANOVA, $F_{1,46}=10.4$, $P=0.002$), while the biomass of the rest of the transects (W, WC, and C stations) were not significantly different between the two studies (ANOVA, $P > 0.1$).

Because regression slopes and elevations were not significantly different between NGoMCS and DGoMB, they were combined to compare with the S GoM data (Fig. 6). Both the N and the S GoM biomasses declined significantly (log-linear) with depth (Table 4a, north, $F_{1,94}=242.7$, $P < 0.001$; south, $F_{1,69}=89.1$, $P < 0.001$). The regression slopes were not significantly different between the N and S GoM (Table 4b, ANCOVA, slope, $F_{1,163}=0.8$, $P=0.37$); however, the regression elevation of the N GoM was significantly higher than the S GoM (elevation, $F_{1,163}=136.8$, $P < 0.001$).

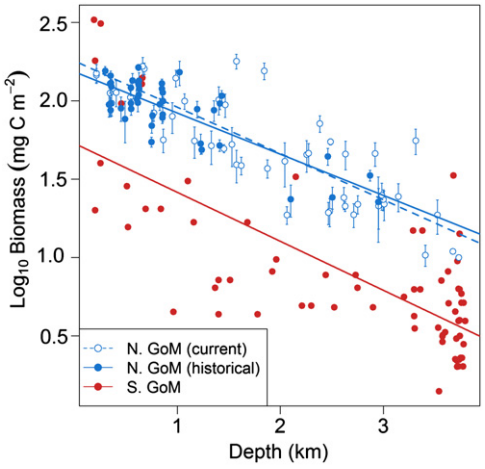

Fig. 6. Log_{10}-transformed organic carbon biomass as functions of water depth for the DGoMB, NGoMCS, and S GoM studies. Linear regressions were conducted on the station averages from core replications. The standard error is shown as error bar. The test statistics of linear regression can be found in Table 4a.

Table 5
Randomized complete block ANOVA on organic carbon biomass for revisited sites between historical NGoMCS and current DGoMB studies. Blocking factor is different sites along the selected transects.

ANOVA	Df1	Df2	SS	MS	F	P
W stations						
Study	1	33	0.04	0.04	2.4	n.s
Block	4	33	2.6	0.6	43.0	****
WC5 and WC12						
Study	1	19	0.1	0.1	1.5	n.s
Block	1	19	0.9	0.9	24.1	****
C stations						
Study	1	88	0.1	0.1	2.2	n.s
Block	4	88	4.3	1.1	17.7	****
S41, S42, and S43						
Study	1	46	0.3	0.3	10.4	***
Block	2	46	3.6	1.8	73.0	****

Significance codes: n.s.: $P \geq 0.1$.
*$P < 0.1$.
**$P < 0.05$.
*** $P < 0.01$.
**** $P < 0.001$.

3.3. Random forest (RF) modeling and standing stock prediction.

A total of 3750 scaling scenarios (for ocean color data) were computed to run Random Forests (RF) analysis on 669 biomass and 640 abundance records. The RF models explained 73.1%–79.2% of the out-of-bag (OOB) biomass data (Fig. 7) and 51.7% to 60.9% of the OOB abundance data (Fig. A1). The ocean color data from direct spatial matching and concurrent to benthic sampling (time lag=0, window=0, catchment=0, Fig. 7) had the lowest fit to the empirical data (lowest R^2). The model performance improved with increasing catchment radius (y axis) and accumulating time (top left to bottom right panels, Fig. 7). The peak performance (highest R^2) had a seasonal time lag (x axis) and appeared to be independent of the larger catchment radius ($>$ 60′ or 1 arc degree). The kernel density distributions of the lag time for the top 10% ($R^2=78.7\pm0.14\%$, $n=375$, Fig. 8a) and top 100 RF models ($R^2=78.9\pm0.11\%$, $n=100$, Fig. 8b) peaked at ~8 to 9 and ~19 to 20 months prior to the sampling month, respectively. The density of the second peak, however, was lower, possibly reflecting a seasonal signal of the first lag time density peak. The density of the accumulating window increased steadily from window=0 to window=5. The catchment radius had the highest density at ~100 to 105′ (~1.7 arc-degrees).

Comparison of the out-of-bag (OOB) predicted and observed biomass from the top 100 RF models (Fig. 8b) is shown in Fig. 9a. The dashed line indicates a perfect fit between the OOB predictions and empirical values. The actual linear fits (solid lines) suggest that the OOB predictions were closer to the empirical data at an intermediate biomass range, but slightly underestimated and overestimated the high (eg. Mississippi Canyon) and low values (e.g. abyssal plain), respectively. When the OOB predictor values were "conditionally" permuted (see methods), water depth caused the greatest increase in prediction mean square error (Fig. 9b), followed by monthly SD of sea surface temperature (sst.sd), monthly mean mixed layer depth (mld.mean), and monthly mean Vertical General Production Model (vgpm.mean), etc. In other words, these were the predictors that influenced the model accuracy the most.

Partial dependence plots on the most influential predictors provided insights on how these variables may affect model predictions (Fig. 10). It appears that the effect of depth was negative and rather continuous on the predicted biomass, except for a relatively stronger response (sharper decline) at ~2000 m (Fig. 10a). The RF model also had the strongest positive response to monthly SD of sea surface temperature between 0.4 and 1.5 °C (Fig. 10b), negative response to mean mixed layer depths from ~13 to 37 m (Fig. 10c), and positive response to mean net primary production from ~200 to 600 mg C m^{-2} day^{-1} (Fig. 10d). The effect of monthly mean mixed layer depth was positive at the shallowest end and then switched to negative as the mixed layer became deeper (Fig. 10c). It is worth noting that only the water depth seems to have lasting influence on the model predictions throughout the entire data range. The influence of other important predictors was mostly concentrated on the lower ranges of the gradients.

Mean predicted biomass and its coefficient of variation (CV) based on the top 100 RF models were computed for the June months from 2000 to 2010 (Figs. A2 and A3). The zoomed-in versions of the yearly mean prediction and CV in the vicinity of *Deepwater Horizon* (DWH) platform are provided in Figs. A4 and A5, respectively. The mean predictions against depth and empirical data are also available in Figs. A6 and A7. Here, we reported the composite images of inter-annual mean and CV for the predicted time series (Fig. 11, data available in File A1).

A total of 96.4 ± 7.93 kt ($n=11$ years) of macrofaunal carbon were estimated for the months of June (from 2000 to 2010) in the GoM basin (cut off from the Yucatan Channel and Straits of Florida) based on summation of predicted cell values (carbon biomass per unit area) × area of a 5′ grid at the equator (86 km^2) × cosine of latitude for the grids (Fig. 11a). Generally, similar biomass values (same colors) occurred in depth bands parallel to isobaths and declined toward the center of the deepest part of the GoM basin. The coefficient of variation (CV), however, was highest in the western central GoM (~25%) and relatively low on much of the continental shelf and upper slope ($<$10%, Fig. 11b). The northern half of the GoM basin shows higher biomass than the southern half of the basin (Fig. 11a).

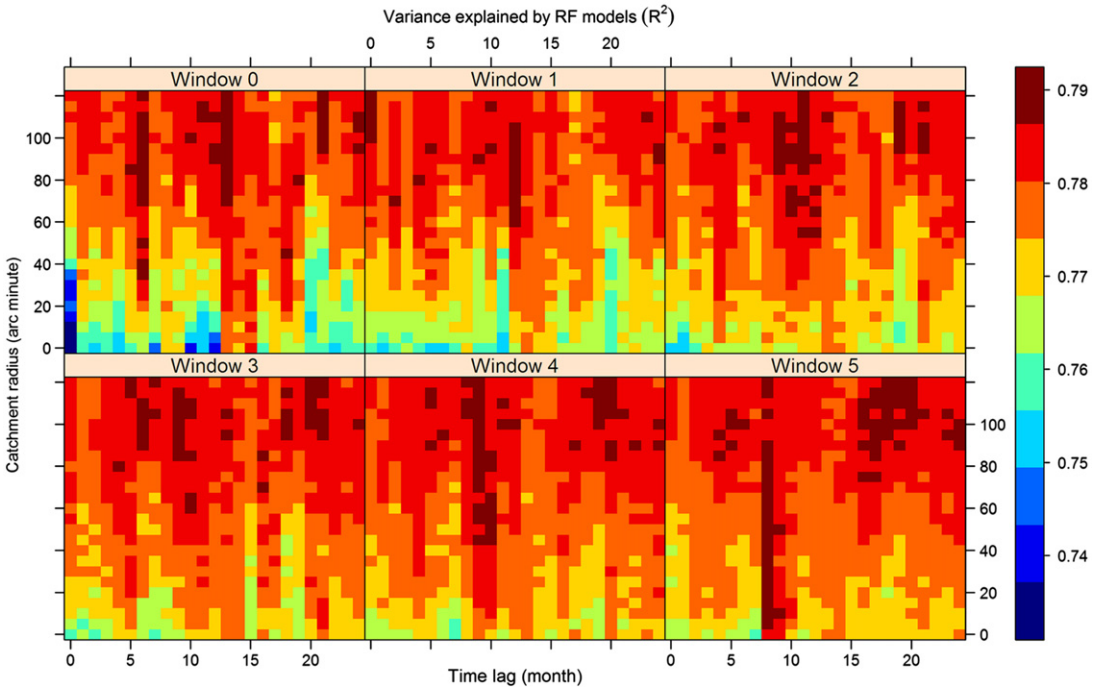

Fig. 7. Performance of Random Forest (RF) models on macrofauna organic carbon biomass based on different lag time, catchment radius, and accumulating window of ocean color data. Color gradient shows the variance explained (R^2) by the RF models.

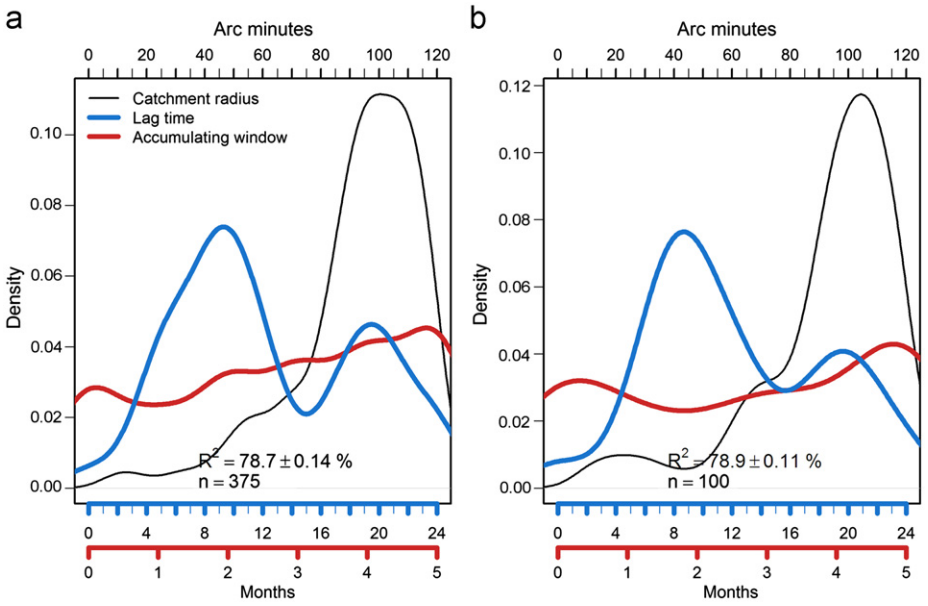

Fig. 8. Kernel density distribution of catchment radius, lag time, and accumulating window for the (a) top 10% and (b) top 100 Random Forest (RF) models (from Fig. 7) on macrofauna organic carbon biomass.

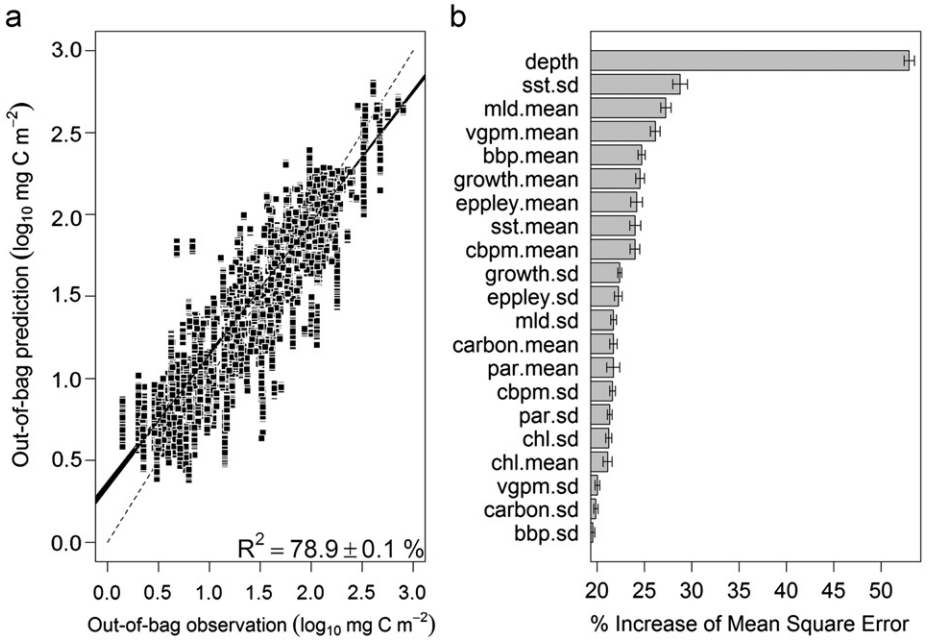

Fig. 9. (a) Out-of-bag (OOB) predicted against observed carbon biomass and (b) mean conditional predictor importance for the top 100 Random Forest (RF) model. Dashed line indicates perfect fit between OOB predictions and empirical values. Solid lines show actual fits between predicted and observed $\log_{10}$ carbon biomass. Bar chart shows the average increase of percent mean square error (MSE) after conditional permutations for the top 100 RF models. Error bars show standard error of the average importance.

The predicted cells north of the Rio Grande River (north of Latitude 26°N) contributed 61.6% of total carbon biomass in merely 36% of GoM grid area. The highest $\log_{10}$ biomass ($\sim$2.5 or 316 mg C m^{-2}) dominated much of the continental shelf of Louisiana and Mississippi with relatively narrow distribution and slightly lower biomass on the shelves of Texas, Florida, and the Mexican states of Yucatan and Campeche (see Fig. 1 for state labels). The lowest $\log_{10}$ biomass (<1 or 10 mg C m^{-2}) occupied much of the Sigsbee and Florida Abyssal Plain near the center of the GoM basin, continental slope of the SW GoM, and the Caribbean basin south of the Yucatan Channel.

High $\log_{10}$ biomass (>2.5 or 316 mg C m^{-2}, Fig. 11c) mostly occurred shallower than 50-m depth (94.3% of cells) but submerged near the head of the Mississippi Canyon (MT1) to $\sim$350-m depth. The $\log_{10}$ biomass between 2.2 and 2.5 (or 158 and 316 mg C m^{-2}) occurred mostly above the 100-m isobath (77.6% of cells) but also submerged to $\sim$1000-m depth on the upper Mississippi Canyon (MT3) and reached as deep as $\sim$1400-m depth to the east of the Mississippi River delta (HiPro). The $\log_{10}$ biomass at the location of the DWH platform (MC252, $\sim$1500-m depth) was predicted to be 2.18 (or 151 mg C m^{-2}) with a coefficient of variation of 5.1% (Fig. 11d). The prediction is somewhat close to the empirical biomass at Stations MT2, HiPro, S35, S36, and S44 (150–178.8 mg C m^{-2}, Table 2).

Detailed examination of reduced models (based on a subset of predictors) is provided in Fig. A8 and A9. Most of the reduced RF

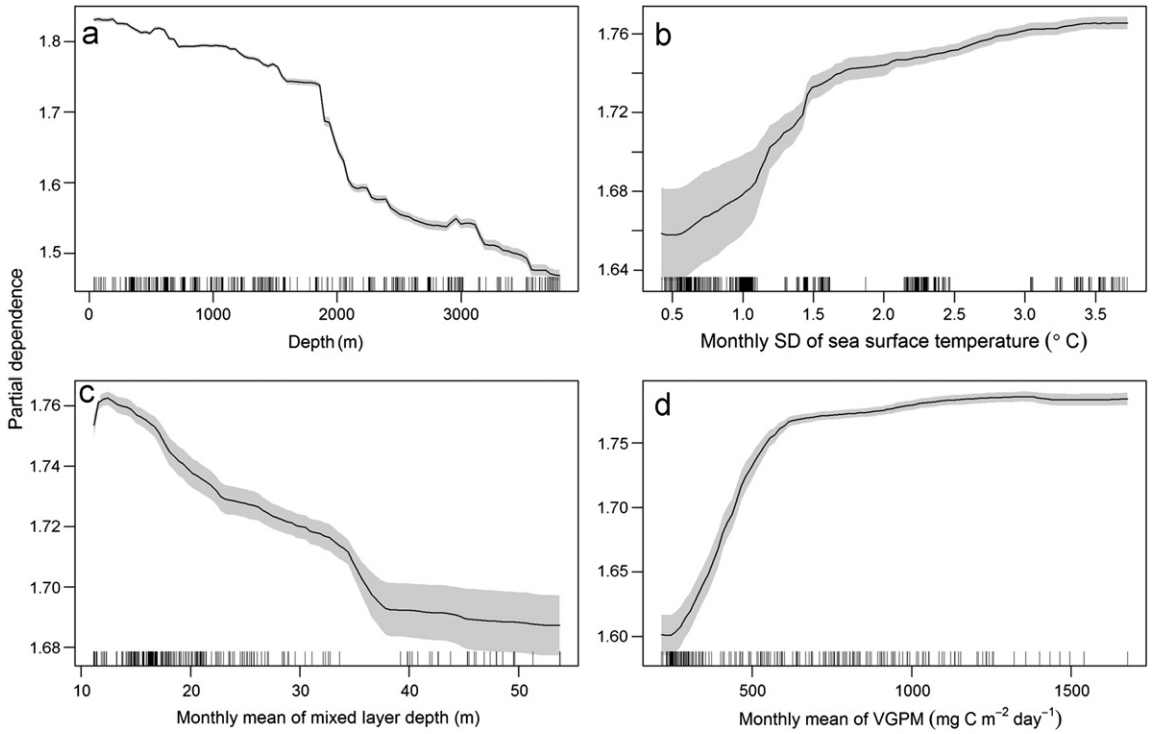

Fig. 10. Mean partial dependence of (a) depth, (b) monthly standard deviation of sea surface temperature, (c) monthly mean of mixed layer depth and (d) monthly mean of Vertical General Production Model (VGPM) for the top 100 Random Forest (RF) models. Shaded area shows 95% confidence interval of the mean. Hash marks show the distribution of predictor values.

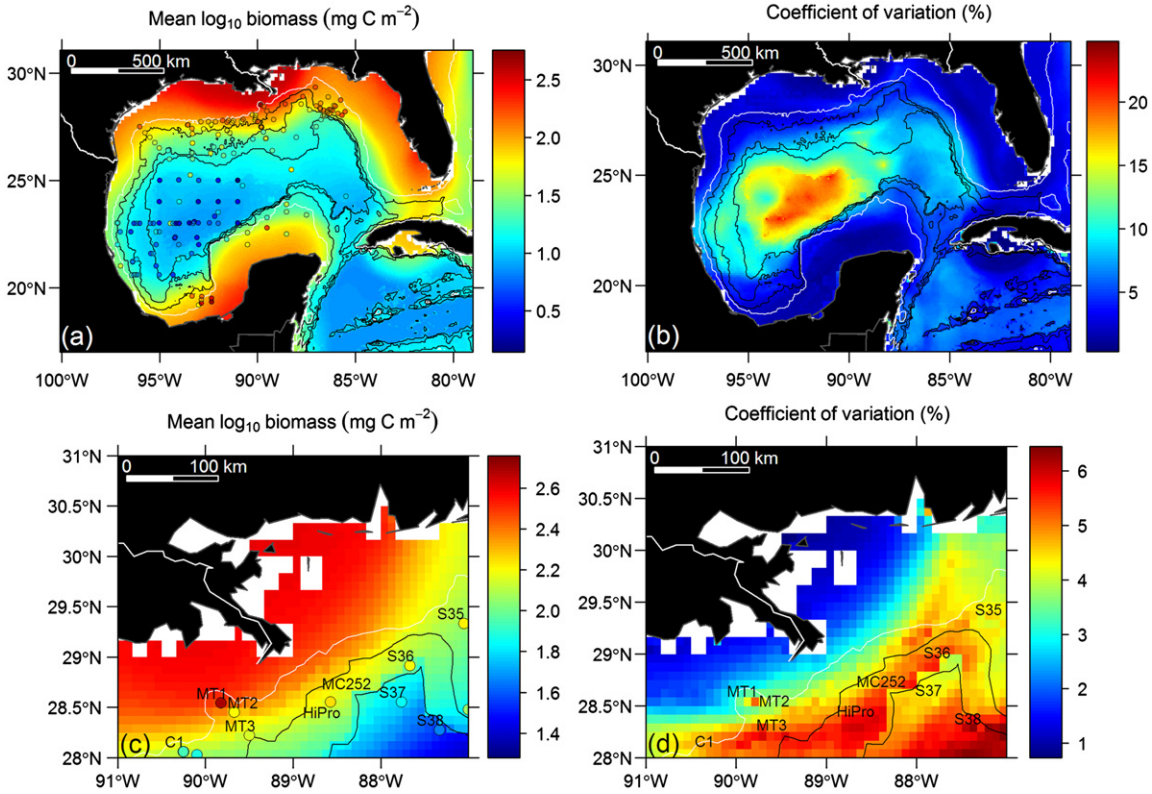

Fig. 11. Random Forest (RF) predictions of macrofauna carbon biomass in the GoM. (a) Inter-annual mean biomass prediction for the June months from 2000 to 2010. Color gradient shows $\log_{10}$ organic carbon biomass (mg C m^{-2}). Color gradient within circle symbols shows the empirical biomass. (b) Coefficient of variation of the inter-annual mean. Color gradient shows standard deviation (SD)/mean × 100 (%). (c) Inter-annual mean biomass prediction in the vicinity of the *Deepwater Horizon* (DWH) oil spill site. MC252 shows the location of DWH platform. (d) Coefficient of variation in the vicinity of the DWH platform.

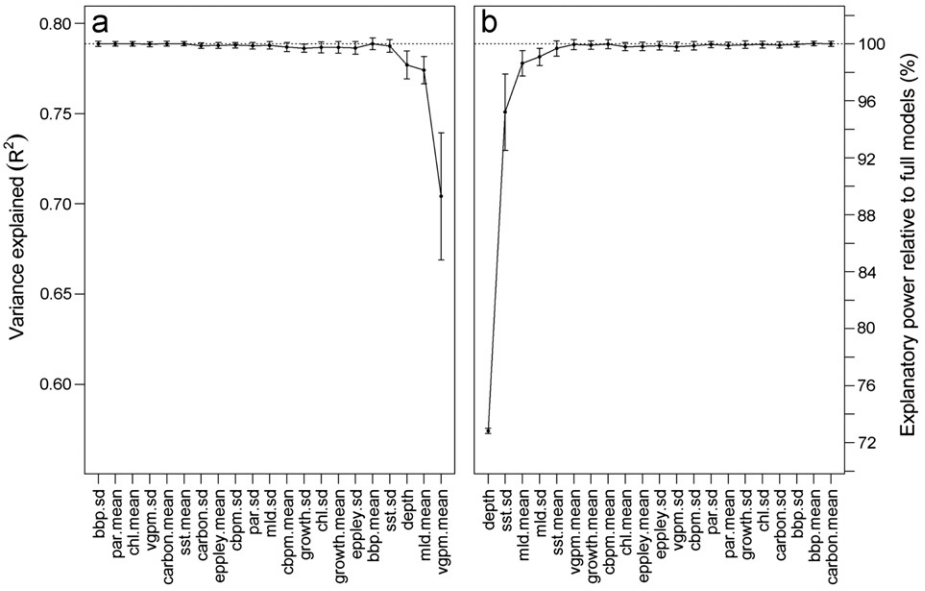

Fig. 12. Mean performance of reduced Random Forest (RF) models based on top 100 scaling scenarios. (a) Step-wise elimination of the least important predictors in the reduced models. The solid circle symbol shows each iteration step. The predictor (on the *x* axis) corresponding to the symbol is removed in the next iteration. (b) Step-wise inclusion of the most important predictors to the reduced model. The solid symbol corresponds to the predictor (on the x axis) being added to the current iteration. Error bar shows standard deviation of the mean performance.

models still maintained more than 98% of the explanatory power relative to the full models (Fig. 12). On the one hand, the model performance (R^2) did not drop dramatically until removing the last few predictors (step-wise elimination, Fig. 12a). On the other hand, the R^2 also did not increase much after the first few predictors were included in the reduced models (step-wise inclusion, Fig. 12b). The SD of R^2 (error bars) on both approaches, however, appears to be smaller when more predictors were included in the reduced models. The error bars are almost negligible when depth is the only predictor, because depth is independent of scaling and always consistent among the selected models.

4. Discussion

4.1. Relationship between standing stocks, body size and energy constraints

Except for bacteria, logarithmic declines of biomass with depth have occurred across all major size groups for soft-bottom communities (Rex et al., 2006; Rowe, 1971; Rowe, 1983; Wei et al., 2010b) and is widely accepted to be caused by an exponential decline of the particulate organic carbon (POC) flux from the euphotic zone to the seafloor (Pace et al., 1987; Rowe, 1971; Suess, 1980). The decline of average macrofaunal body size (biomass/abundance) with depth, however, requires careful interpretation, because the size variation in fact indicates a change of relative abundance among taxa, as the variability within taxa was not measured in this study; hence, a more appropriate statement should be that the taxonomic composition of macrobenthos shifts to the smaller taxa with depth. This observation was supported by a shift of dominance (in terms of abundance) from large sensu-stricto macrofauna on the upper slope to nematodes, harpacticoids, and ostracodes on the lower slope and abyssal plain.

It has been postulated that small body size has the advantage to conserve energy and maintain viable populations in the food-limited deep sea (Rex et al., 2006; Thiel, 1975; Wei et al., 2010b) as opposed to being large and benefiting from competition, resource exploitation, metabolic efficiency, and predation avoidance (McClain et al., 2009). The upper slope of the N GoM may favor the larger taxa such as polychaetes and amphipods because of abundant resources, while the meager POC input on the abyssal plain favor smaller taxa, such as nematodes, harpacticoids, and ostracodes (Biggs et al., 2008; Morse and Beazley, 2008; Rowe et al., 2008a).

Evidence supporting this speculation comes from outliers in the standing stock-depth regressions (Figs. 3 and 4). The head of Mississippi Canyon (Station MT1) had extremely high abundance and biomass with almost no nematodes, harpacticoids, and ostracodes, presumably because of competitive exclusion by the dominant amphipod *A. mississippiana*. The latter, we presume, 'bloomed' due to the POC input to the seafloor (77.7 mg C m^{-2} day^{-1}), the highest estimated among the DGoMB sampling sites (Biggs et al., 2008). Moreover, the macrofaunal biomass only exceeded the meiofaunal (metazoan + foraminiferal) biomass at this location (Baguley et al., 2008; Rowe et al., 2008b). In fact, the total meiofauna biomass at MT1 was still among the highest in the DGoMB sites (Baguley et al., 2008), suggesting that only the largest nematodes, harpacticoids, and ostracodes (retained by 300-μm sieve) were lacking. It may be possible that these meiofaunal taxa were out-competed by the macrofaunal taxa. The tube-dwelling, suspension feeding amphipod, *A. mississippiana*, appear to be especially adapted to the abundant settling organic matters at MT1 (Soliman and Wicksten, 2007). Their dense tube mats carpeted the seafloor of MT1 (personal observation) probably providing protection against the strong near-bottom currents commonly occurring in the upper canyon (Ross et al., 2009) and also likely limiting the living space of the smaller macrofauna.

Another intriguing outlier, Station HiPro, located just 27-km southwest of the *Deepwater Horizon* blowout site (Fig. 1), also showed high biomass, large average size, and high abundance of the sensu-stricto macrofauna at ~1600 m below the sea surface, presumably associated with upwelling nutrient-rich water onto the upper slope or entrainment of the Mississippi River water. The species composition of Station HiPro was more closely related to the shallow shelf-break communities than other stations of similar depths (Wei et al., 2010a). Elevated amounts of POC input

via lateral advection from the surrounding shelf and slope may add organic detritus to support this benthic community, since the satellite-based estimates (Biggs et al., 2008) did not suggest excessive input of surface-derived POC to the bottom. The surface productivity at the Station HiPro was high and comparable to the shelf-break sites but delivery estimates were reduced by the depth-exponential-decay equation (Pace et al., 1987) applied to convert surface primary production to export POC flux to the seafloor (Biggs et al., 2008).

At ~3300 m below the sea surface, the deep Mississippi sediment fan (Station S5) was a favorable habitat for macrofaunal nematodes, harpacticoids, and ostracodes. Their abundances were 2–6 times more than at other sites on the abyssal plain (Table A4). The sediment fan also favored bivalve and aplacophoran mollusks, with a 5 to 6-fold increase in abundance over the other abyssal sites. High total standing stocks, with a species composition more related to deep continental slope communities (Wei et al., 2010a) suggests that the macrobenthos at the Station S5 was influenced by the slumping or down-slope movements of organic-rich sediments from the Mississippi River and surrounding shelves through the submarine canyon (Wei et al., 2010a), in addition to vertical particle flux (Biggs et al., 2008).

4.2. Hypotheses testing

Based on ANCOVA results, we rejected Null Hypothesis 1. The Mississippi Canyon was unique in terms of the overall level and the rate of declining biomass with depth. Compared to the continental slopes in the NW or NE GoM, the biomass was significantly elevated on the upper and mid sections of the Mississippi Canyon. Submarine canyons are potential conduits of sediments and organic materials from the continental shelf to the deep basin. River flushing, storm surges, earthquakes, or down-slope currents can cause mass wasting of sediments along the canyon axis (Gardner, 1989; Santschi and Rowe, 2008). During the DGoMB trawl survey in year 2000, macrophyte debris, including the water hyacinth (*Eichhornia crassipes*), *Sargassum* sp., and wood fragments of all sizes, were found on the seafloor of the shallow head of the Mississippi Canyon (Wei et al., 2012). The water hyacinths (23 clumps, length ca. 15 cm) were only found at the canyon head, presumably originating from the river. High macrofaunal biomass associated with the enrichments of macrophyte debris has also been reported elsewhere in submarine canyons (De Leo et al., 2010; Vetter and Dayton, 1998). It is possible that the high macrofaunal biomass was a function of rapidly accumulating macrophytes and organic materials exported from the Mississippi River and adjacent continental shelf. The extremely high biomasses at the canyon head declined rapidly along the axis toward the lower section of the canyon and its sediment fan (Station MT6), where the biomass was equal to or lower than the other continental slope transects. Interestingly, a large quantity of cobble-sized, reddish-colored sedimentary rocks, so called "iron stones", have also been found in the area from box corers, trawls, and bottom photographs (Pequegnat, 1983; Rowe and Kennicutt, 2009; Wei et al., 2012). It has been suggested that this "iron stone" could be formed following massive submarine slumping of unstable continental margin sediments (Bryant et al., 1991; Rowe et al., 2008b; Santschi and Rowe, 2008). Strong bottom currents below the Florida and Sigsbee Escarpment were also evident in the bottom photographs (Rowe and Kennicutt, 2009) and could affect the pattern of macrofaunal zonation (Wei et al., 2010a); however, it is unclear if this low biomass was linked to the "iron stones", strong bottom currents, or both.

The Central Transect maintained high biomass at mid to lower slope depths. During the NGoMCS sampling, the peak macrofaunal abundance occurred at 620-m and 1400-m depths on the Central Transect. The cause was attributed to possible hydrocarbon seeps in the proximity of Station C7 (~1000-m depth, Pequegnat et al., 1990; Rowe and Kennicutt, 2009). Cold seeps are known to support dense macrofaunal communities throughout the continental margins of the world's oceans (Sibuet and Olu, 1998). Heterotrophic macrobenthos living in the immediate vicinity of seeps could benefit from the abundant carbon source in the food-limited deep-sea; however, the enhancement appears to be localized (Carney, 1994). No apparent enhancement of surface production or export POC flux was observed on the Central Transect or on the abyssal plain at Station S5 (Biggs et al., 2008). Additional sources of detritus may be a complex interaction between the down-slope sediment transport (Balsam and Beeson, 2003; Santschi and Rowe, 2008) and westward bottom currents (Hamilton and Lugo-Fernandez, 2001; Oey and Lee, 2002) shifting expected biomass-enrichment west away from the axis of Mississippi Canyon.

Null Hypothesis 2 was rejected. The De Soto Canyon harbored significantly greater macrofaunal biomass than the slope transects. In contrast to the Mississippi Canyon, the De Soto Canyon does not receive riverine inputs directly and has been an area of non-deposition with little evidence for recent sediment transport (Bryant et al., 1991). However, similar to HiPro, the surface water of De Soto Canyon is affected by warm slope eddies (WSEs), which entrain low salinity-high chlorophyll Mississippi River water (Jochens and DiMarco, 2008). The WSEs advect the turbid "green-water" plume seaward and enhance the surface primary production and associated export flux of POC to the deepwater of NE GoM (Biggs et al., 2008). The biomass-depth regression slope for the De Soto Canyon, however, was not statistically different from the regression slopes of other continental slope transects, suggesting that similar processes may govern the remineralization of sinking phytodetrital carbon despite surface water being more productive over the De Soto Canyon.

Null Hypothesis 3 and 4 were not rejected. Neither the steep Florida Escarpment nor the small continental slope basins on the NW GoM slope had a significant effect on macrofaunal biomass. Despite an abrupt 2200-m depth drop along the Florida slope, the decline of biomass still followed a general depth trend similar to the NW GoM slope. It was hypothesized that the base of the Florida Escarpment (Station S41) might experience organic enrichment due to the steep escarpment and its proximity to productive continental shelf; nonetheless, our observations suggest that water depth, not distance away from the shelf, controlled the pattern of declining biomass. The numerous small slope basins in the north central GoM were also hypothesized to funnel or trap organic materials during frequent gravity slumping and density flows on the continental margin of NW GoM (Bryant et al., 1991), and in fact, after removing the depth effect by ANCOVA, we did observe a slight, but not statistically significant enrichment of carbon biomass within the basin relative to the non-basin slope.

Null Hypothesis 5 was not rejected. No significant change in macrofaunal biomass was observed between the historical and current sampling in the N GoM. It should be noted that this conclusion is based on the assumption that the average sizes of major taxonomic groups were not different between the two studies. The sampling for both studies used the same sieve and corer design; however, the DGoMB biomass was estimated based on a larger core area (0.2 m^2 vs. 0.06 m^2 for NGoMCS).

Null Hypothesis 6 was rejected. Macrofaunal biomass on the continental margins of N GoM was significantly higher than the S GoM, even though a slightly smaller sieve size was used in the S GoM (250 μm vs. 300 μm in N GoM). The north-south variation is probably a function of surface primary production and associated export POC flux. In the NGoM the world's third largest drainage

basin, the Mississppi-Atchafalaya Rivers discharge 530 billion m^3 of freshwater and 210 megatons of sediments annually onto the continental shelf of the N GoM (Cai and Lohrenz, 2010). The nutrient-laden Mississippi River plume interacts with shelf/slope eddies (Biggs et al., 2008). Although upwelling occurs along the edges of the Loop Current with concomitant high surface productivity along the Florida Escarpment and Campeche Bank (Jochens and DiMarco, 2008), the S GoM is dominated by low productivity water from the central Caribbean that enters the GoM via the Yucatan Strait (Jochens and DiMarco, 2008; Lohrenz et al., 1999; Wiseman and Sturges, 1999). This water mass conserves its hydrographic properties for a prolonged period of time (Wiseman and Sturges, 1999) with resulting low benthic biomass in the southern GoM.

4.3. Random forests and biomass predictions

Estimates of macrofaunal abundance are sensitive to artifacts such as gear design, sieve size, fragmentation of specimens, and human sorting error (Gage and Bett, 2005; Gage et al., 2002; Pavithran et al., 2009). Our composite dataset was collected by multiple devices with slightly different sieve sizes between the N and S GoM; hence, the comparisons of animal density among studies were subjected to gear efficacy and may not fully reflect the variations of standing stocks. Given that most of the total macrofaunal biomass is concentrated in large, less abundant animals, biomass is better suited and more dependable for assessing the standing stocks among studies (Rowe, 1983). This may be why the Random Forest (RF) analysis explained more variability for the biomass than for abundance. In fact, one might argue that our predicted biomass may better represent the large-scale patterns in standing stocks than the empirical measurements, because the new ocean color and bathymetry data for making the predictions were always measured consistently and simultaneously across the entire region. It is also evident that within the DGoMB study, the bathymetric pattern of biomass did not completely follow the pattern of density due to variation of animal size with depth. The sensu-stricto density, on the other hand, was a better representation of the biomass.

Despite exhaustive searches for optimal scaling on ocean color data, water depth was still the best predictor for macrofaunal biomass, suggesting that it is a better surrogate for benthic food supply or utilization of energy through the mid-water food web (Rex et al., 2006; Rowe, 1983; Rowe and Menzel, 1971; Rowe et al., 1974; Wei et al., 2010b). Our optimal lag time (first lag time density peak in Fig. 8b) agreed with empirical time-series in the abyssal NE Pacific, in which the variation of macrofauna abundance lagged behind the surface climate events by 8–9 months (Ruhl et al., 2008; Smith et al., 2009). However, owing to the broad range of our sampling, complex circulation, and unknown animal response time (recruitment, growth, etc.), it is impossible to determine a precise scale that reflects the POC effects hundreds or thousands of meters below the sea surface. The time lags for the POC delivery and animal response could vary among locations and our approach could only describe an average scaling for the entire system. As a result, the improvement of model performance (R^2) from the simulations was only moderate ($\sim$8.3%) with the density distribution of the top models skewing toward the longer accumulation and larger catchment area of ocean color data. Regardless, the purpose of these simulations was to optimize the models rather than to determine the exact scaling between the benthos and climatic events.

Besides error inherited from sample processing and predictor scaling, the unexplained variability in the macrofaunal biomass may also reflect energy sources not directly measureable, such as the lateral or horizontal transport of carbon into or out of a habitat (Rowe et al., 2008a), hydrocarbon inputs from the cold seeps (Cordes et al., 2009), and accumulation of macrophytes on the seafloor and in the submarine canyon (Wei et al., 2012). Other factors that are physiologically important such as bottom water temperature (Narayanaswamy and Bett, 2011), dissolved oxygen (Levin, 2003), and export POC flux (Johnson et al., 2007) were not included, because the available global data (Levitus, 2010) or models (Dunne et al., 2007; Yool et al., 2009) were not of sufficient temporal and spatial resolution. A broader global scale analysis (Wei et al., 2010b), however, demonstrated that ocean color data and bathymetry alone can explain much of the observed stock variances. For RF, as with other modeling methods, collinearity between independent variables raises issues that need to be addressed. Specifically, correlation among predictors may result in inflated estimates of predictor importance (Strobl et al., 2008). The predictive performance of RF, however, is not sensitive to correlative predictors because of the randomized predictor selections (Breiman, 2001). In the previous global synthesis (Wei et al., 2010b), we did not consider the predictor collinearity because the focus had been on generating accurate seafloor biomass maps. For studies focusing on relative roles or mechanisms of independent variables, however, we suggest conditional predictor importance (Smith et al., 2011; Strobl et al., 2008) as implemented in this study and by others (Pitcher et al., 2012) to alleviate the inflationary effect of correlations.

Even though we did not include biomass observations from the continental shelf of the N GoM and the deep Caribbean Basin, our predictions of the areas ($\log_{10}$ mg C m^{-2}, Fig. 11a) are comparable or at least not far from the literature values (Table A4) on the shelves of the Texas (2.1 ± 0.27, $n=10$, Gettleson, 1976) and Mississippi (1.62 ± 0.34, $n=7$, Rowe et al., 1974), as well as in the deep Caribbean basin (0.8 ± 0.39, $n=3$, Richardson and Young, 1987), suggesting that the extrapolation of predictions may be appropriate. Nevertheless, it is worth noting that Gettleson (1976) and Rowe et al. (1974) used a van Veen grab and coarser sieves (500 and 420 μm, respectively); therefore, their estimates could be slightly lower than our predictions based on sampling with a GOMEX box corer and 300-μm sieve (Gage and Bett, 2005).

Our modeling approach has potential to now-cast or even forecast the benthic standing stocks from the surface conditions; however, a training dataset from a time-series study that incorporates seasonal variability would be needed. For example, $\sim$83% of the biomass data in the GoM were collected in early summer and only $\sim$15% were in the winter. In fact, most of the winter sampling focused on C Transect during the NGoMCS study with a few samples on the Campeche bank during the OGMEX study (Fig. 1). In this analysis, the utility of biomass models based on subsets of predictors was also explored. As implied in the quote "*all models are wrong, but some are useful*" (Box and Draper, 1987), the simplest model might be the most useful one. This is especially true when we try to assess the potential effects of climate change on the deep-sea benthos, because it is already difficult to generate the future climate scenario for a single predictor (e.g. sea surface temperature), let alone come up with the scenarios for 21 interacting variables. The potential effect of climate change can then be visualized by the predictor partial dependences. For example, our current full model suggests that warming of the surface ocean (if changing the temporal variability of sea surface temperature) may shift the distribution of macrofauna biomass (Fig. 10b).

We estimated that the sediments underneath the DWH platform (MC252) were a biomass hotspot ($\log_{10}$ biomass$=2.18 \pm 5.1\%$ or 117 to 196 mg C m^{-2}). At $\sim$1500-m depth, the macrofaunal biomass could be comparable to that of the shallow continental shelf ($\sim$100-m depth) in the N GoM. The hydrocarbons released by the DWH oil spill are also an energy source and

eventually will be degraded and assimilated into the aquatic food web. If everything ultimately falls to the seafloor, can we see a surge of benthic biomass similar to what has been observed at the head of the Mississippi Canyon? The amount of hydrocarbons released during the spill (up to 500 kt, Joye et al., 2011), however, was relatively small compared to the annual organic carbon export from the Mississippi River (on the order of megatons per years, Cai and Lohrenz, 2010). Another possibility could be the loss of environmentally sensitive species during the initial spill followed by succession of opportunistic, pollution-resilient species during the recovery stage (Kingston, 2002). Our results predict a baseline condition of the sediment-dwelling macrobenthos that may be under immediate or long-term impacts of the DWH oil spill. It is necessary to revisit these historical sites using similar sampling methods (e.g. GOMEX Box Core, 300-μm sieve) to make sensible comparison for post-spill effect assessment.

Acknowledgements

We thank Fain Hubbard who participated in the original NGoMCS study as a graduate student and oversaw the day-to-day DGoMB macrofauna sorting activity. He passed away shortly after completion of the DGoMB project; however, his influence and imprint has been long recognized in the numerous publications on the deep GoM benthos. We also thank Archie Ammons, Lindsey Loughry, Min Chen, Matt Ziegler, Xiaojia Chen, and Yuning Wang for many hours at sea and sample sorting in the TAMU lab. We are grateful to Jay Rooker, Dan Thornton, Antonietta Quigg, Andy Gooday, Paul Snelgrove, Ryan Stanley, and four anonymous reviewers for their invaluable discussions with C–L Wei, as well as comments and suggestions on the manuscript. We also thank Michele Durand for managing the CoML Fresh Biomass Synthesis Project. The NGoMCS and DGoMB study were funded by the US Department of Interior, Minerals Management Service (Contract 30991), now Bureau of Ocean Energy Management (BOEM). The UNAM field work was supported by *Factores que definen la variabilidad de la diversidad biológica y biomasa béntica en el mar profundo del Golfo de México Convocatoria del Programa de Apoyo a Proyectos de Investigación e Innovación Tecnológica* (PAPIIT IN207410). This paper is a contribution of the Continental Margin Ecosystems (COMARGE) and Cross-Project Synthesis of the Census of Marine Life (CoML) supported by the Alfred P. Sloan Foundation. Data analyses were partly supported by Canadian Healthy Oceans Network (CHONe) through a fellowship to C–L Wei.

Appendix A. Supporting information

Supplementary data associated with this article can be found in the online version at http://dx.doi.org/10.1016/j.dsr.2012.07.008.

References

Adcroft, A., Hallberg, R., Dunne, J.P., Samuels, B.L., Galt, J.A., Barker, C.H., Payton, D., 2010. Simulations of underwater plumes of dissolved oil in the Gulf of Mexico. Geophys. Res. Lett. 37 (18), L18605.

Arredondo, I., 2011. Variabilidad de la biomasa de la comunidad bentónica de la macroinfauna de la Planicie Abisal Sigsbee en el sector central del Golfo de México. Universidad Nacional Autónoma de México (UNAM), D.F. México.

Asper, V.L., Deuser, W.G., Knauer, G.A., Lohrenz, S.E., 1992. Rapid coupling of sinking particle fluxes between surface and deep ocean waters. Nature 357 (6380), 670–672.

Baguley, J.G., Montagna, P.A., Hyde, L.J., Rowe, G.T., 2008. Metazoan meiofauna biomass, grazing, and weight-dependent respiration in the Northern Gulf of Mexico deep sea. Deep-Sea Res. II 55 (24–26), 2607–2616.

Balsam, W.L., Beeson, J.P., 2003. Sea-floor sediment distribution in the Gulf of Mexico. Deep-Sea Res. Part I: Oceanographic Res. Papers 50 (12), 1421–1444.

Bianchi, T.S., Allison, M.A., Canuel, E.A., Corbett, D.R., McKee, B.A., Sampere, T.P., Wakeham, S.G., Waterson, E., 2006. Rapid export of organic matter to the Mississippi Canyon. Eos, Trans. Am. Geophys. Union 87 (50), http://dx.doi.org/10.1029/2006EO500002. (50).

Biggs, D.C., Hu, C., Müller-Karger, F.E., 2008. Remotely sensed sea-surface chlorophyll and POC flux at Deep Gulf of Mexico Benthos sampling stations. Deep-Sea Res. II 55 (24–26), 2555–2562.

Bivand, R.S., Pebesma, E.J., Gomez-Rubio, V., 2008. Applied Spatial Data Analysis with R. Springer, New York.

Boland, G.S., Rowe, G.T., 1991. Deep-sea benthic sampling with the GOMEX box corer. Limnol. Oceanogr. 36 (5), 1015–1020.

Box, G.E.P., Draper, N.R., 1987. Empirical model-building and response surfaces. John Wiley & Sons, Oxford.

Breiman, L., 2001. Random forests. Mach. Learn. 45, 5–32.

Bryant, W.R., Lugo, J., Cordova, C., Salvador, A., 1991. Physiography and bathymetry. In: Salvador, A. (Ed.), The Gulf of Mexico Basin. Geological Society of America, Boulder, pp. 13–30.

Cai, W.-J., Lohrenz, S.E., 2010. The Mississippi River plume and adjacent margin in the Gulf of Mexico. In: Liu, K.-K., Atkinson, L., Quiñones, R.A., Talaue-McManus, L. (Eds.), Carbon and nutrient fluxes in continental margins: a global synthesis. Springer, Berlin, Germany, pp. 406–423.

Camilli, R., Reddy, C.M., Yoerger, D.R., Van Mooy, B.A.S., Jakuba, M.V., Kinsey, J.C., McIntyre, C.P., Sylva, S.P., Maloney, J.V., 2010. Tracking Hydrocarbon Plume Transport and Biodegradation at Deepwater Horizon. Science 330 (6001), 201–204.

Carney, R.S., 1994. Consideration of the oasis analogy for chemosynthetic communities at Gulf of Mexico hydrocarbon vents. Geo-Mar. Lett. 14 (2), 149–159.

Coleman, J., Baker, J., Cooper, C., Fingas, M., Hunt, G., Kvenvolden, K., Michel, K., Michel, J., McDowell, J., Phinney, J., Pond, R., Rabalais, N., Roesner, L., Spies, R.B., Walker, D., Merrill, J., Dandelski, J., Greene, D., Saito, J.P., Etkin, D.S., Tait, A.M., Miller, J., 2003. Oil in the Sea III: Inputs, Fates, and Effects. National Academies Press, Washington, D.C.

Conover, W.J., 1999. Practical Nonparametric Statistics. Wiley, New York.

Conover, W.J., Iman, R.L., 1982. Analysis of covariance using the rank transformation. Biometrics 38 (3), 715–724.

Cordes, E.E., Bergquist, D.C., Fisher, C.R., 2009. Macro-ecology of Gulf of Mexico cold seeps. Ann. Rev. Marine Sci. 1 (1), 143–168.

Crone, T.J., Tolstoy, M., 2010. Magnitude of the 2010 Gulf of Mexico oil leak. Science 330 (6004), 634.

De Leo, F.C., Smith, C.R., Rowden, A.A., Bowden, D.A., Clark, M.R., 2010. Submarine canyons: Hotspots of benthic biomass and productivity in the deep sea. In: Proceedings of the Royal Society B: Biological Sciences 277 (1695), 2783–2792.

Dean, H., 2008. The use of polychaetes (Annelida) as indicator species of marine pollution: A review. Revista de Biología Tropical 56 (4), 11–38.

Dunne, J., Sarmiento, J., Gnanadesikan, A., 2007. A synthesis of global particle export from the surface ocean and cycling through the ocean interior and on the seafloor. Global Biogeochem Cycles 21, GB4006.

Ellis, N., Smith, S.J., Pitcher, C.R., 2012. Gradient forests: calculating importance gradients on physical predictors. Ecology.

Escobar-Briones, E., Estrada Santillán, E.L., Legendre, P., 2008a. Macrofaunal density and biomass in the Campeche Canyon, Southwestern Gulf of Mexico. Deep-Sea Res. II 55 (24–26), 2679–2685.

Escobar-Briones, E.G., Díaz, C., Legendre, P., 2008b. Meiofaunal community structure of the deep-sea Gulf of Mexico: Variability due to the sorting methods. Deep-Sea Res. II 55 (24–26), 2627–2633.

Escobar-Briones, E.G., Soto, L.A., 1997. Continental shelf benthic biomass in the western Gulf of Mexico. Cont. Shelf Res. 17 (6), 585–604.

Fodrie, F.J., Heck Jr., K.L., 2011. Response of coastal fishes to the Gulf of Mexico oil disaster. PLoS One 6 (7), e21609.

Friedman, J.H., 2001. Greedy function approximation: a gradient boosting machine. Ann. Statist., 1189–1232.

Gage, J., Bett, B., 2005. Deep-sea benthic sampling. In: Eleftheriou, A., McIntyre, A. (Eds.), Methods for the Study of the Marine Benthos. Blackwell, Oxford, UK, pp. 273–325.

Gage, J.D., Hughes, D.J., Vecino, J.L.G., 2002. Sieve size influence in estimating biomass, abundance and diversity in samples of deep-sea macrobenthos. Mar. Ecol. Prog. Ser. 225, 97–107.

Gage, J.D., Tyler, P.A., 1991. Deep-sea biology: A natural history of organisms at the deep-sea floor. Cambridge University Press, Cambridge.

Gallaway, B.J., 1988. Northern Gulf of Mexico continental slope study, final report: year 4. Volume II: Synthesis report. US Department of the Interior, Minerals Management Service, Gulf of Mexico OCS Regional Office, New Orleans, LA., p. 318.

Gardner, W.D., 1989. Baltimore Canyon as a modern conduit of sediment to the deep sea. Deep-Sea Res. I Oceanographic Res. Papers 36 (3), 323–358.

Gerlach, S., Hahn, A., Schrage, M., 1985. Size spectra of benthic biomass and metabolism. Mar. Ecol. Prog. Ser. 26, 161–173.

Gesteira, J.L.G., Dauvin, J.C., 2000. Amphipods are good bioindicators of the impact of oil spills on soft-bottom macrobenthic communities. Mar. Pollut. Bull. 40 (11), 1017–1027.

Gettleson, D.A., 1976. An ecological study of the benthic meiofauna and macroinfauna of a soft bottom area on the Texas outer continental shelf Ph.D Thesis, Texas A&M University, College Station.

Graham, W.M., Condon, R.H., Carmichael, R.H., D'Ambra, I., Patterson, H.K., Linn, L.J., Hernandez, F.J., 2010. Oil carbon entered the coastal planktonic food web during the Deepwater Horizon oil spill. Environ. Res. Lett. 5 (4), 045301.

Grassle, J.F., Elmgren, R., Grassle, J.P., 1981. Response of benthic communities in merl experimental ecosystems to low level, chronic additions of No. 2 fuel oil. Mar. Environ. Res. 4 (4), 279–297.

Hamilton, P., Lugo-Fernandez, A., 2001. Observations of high speed deep currents in the northern Gulf of Mexico. Geophys. Res. Lett. 28 (14), 2867–2870.

Hazen, T.C., Dubinsky, E.A., DeSantis, T.Z., Andersen, G.L., Piceno, Y.M., Singh, N., Jansson, J.K., Probst, A., Borglin, S.E., Fortney, J.L., Stringfellow, W.T., Bill, M., Conrad, M.E., Tom, L.M., Chavarria, K.L., Alusi, T.R., Lamendella, R., Joyner, D.C., Spier, C., Baelum, J., Auer, M., Zemla, M.L., Chakraborty, R., Sonnenthal, E.L., D'haeseleer, P., Holman, H.-Y.N., Osman, S., Lu, Z., Van Nostrand, J.D., Deng, Y., Zhou, J., Mason, O.U., 2010. Deep-sea oil plume enriches indigenous oil-degrading bacteria. Science 330 (6001), 204–208.

Hemmer, M.J., Barron, M.G., Greene, R.M., 2011. Comparative toxicity of eight oil dispersants, Louisiana sweet crude oil (LSC), and chemically dispersed LSC to two aquatic test species. Environ. Toxicol. Chem., 2011, Article first published online: 19 AUG.

Huitema, B.E., 1980. Analysis of Heterogeneous Regression Case: Johnson-Neyman Technique., The analysis of covariance and alternatives, pp. 271–296, (Chapter 13).

Jochens, A.E., DiMarco, S.F., 2008. Physical oceanographic conditions in the deepwater Gulf of Mexico in summer 2000–2002. Deep-Sea Res. II 55 (24–26), 2541–2554.

Johnson, N.A., Campbell, J.W., Moore, T.S., Rex, M.A., Etter, R.J., McClain, C.R., Dowell, M.D., 2007. The relationship between the standing stock of deep-sea macrobenthos and surface production in the western North Atlantic. Deep-Sea Res. I 54 (8), 1350–1360.

Joye, S., MacDonald, I., 2010. Offshore oceanic impacts from the BP oil spill. Nat. Geosci. 3 (7) 446–446.

Joye, S.B., MacDonald, I.R., Leifer, I., Asper, V., 2011. Magnitude and oxidation potential of hydrocarbon gases released from the BP oil well blowout. Nat. Geosci. 4, 160–164.

Kessler, J.D., Valentine, D.L., Redmond, M.C., Du, M., Chan, E.W., Mendes, S.D., Quiroz, E.W., Villanueva, C.J., Shusta, S.S., Werra, L.M., Yvon-Lewis, S.A., Weber, T.C., 2011. A persistent oxygen anomaly reveals the fate of spilled methane in the deep Gulf of Mexico. Science 331 (6015), 312–315.

Kingston, P.F., 2002. Long-term environmental impact of oil spills. Spill Sci. Technol. Bull. 7 (1–2), 53–61.

Kujawinski, E.B., Kido Soule, M.C., Valentine, D.L., Boysen, A.K., Longnecker, K., Redmond, M.C., 2011. Fate of dispersants associated with the Deepwater Horizon oil spill. Environ. Sci. Technol. 45 (4), 1298–1306.

Lehr, W., Bristol, S., Possolo, A., 2010. Oil budget calculator Deepwater Horizon. The Federal Interagency Solutions Group, Oil Budget Calculator Science and Engineering Team, National Incident Command, p. 217.

Levin, L., 2003. Oxygen minimum zone benthos: adaptation and community response to hypoxia. Oceanogr. Mar. Biol.: Ann. Rev. 41.

Levin, L.A., Sibuet, M., 2012. Understanding continental margin biodiversity: a new imperative. Ann. Rev. Mar. Sci. 4 (1), 79–112.

Levitus, S. (Ed.), 2010. World Ocean Atlas 2009. NOAA Atlas NESDIS 68-71. U.S. Government Printing Office, Washington, D.C., US.

Liaw, A., Wiener, M., 2002. Classification and regression by randomForest. R News 2 (3), 18–22.

Lohrenz, S.E., Wiesenburg, D.A., Arnone, R.A., Chen, X., 1999. What controls primary production in the Gulf of Mexico. In: Kumpf, H., Steidinger, K., Sherman, K. (Eds.), The Gulf of Mexico large marine ecosystem: Assessment, sustainability and management. Blackwell Science, Malden, MA, pp. 151–170.

Lu, Z., Deng, Y., Van Nostrand, J.D., He, Z., Voordeckers, J., Zhou, A., Lee, Y.-J., Mason, O.U., Dubinsky, E.A., Chavarria, K.L., Tom, L.M., Fortney, J.L., Lamendella, R., Jansson, J.K., D'Haeseleer, P., Hazen, T.C., Zhou, J., 2012. Microbial gene functions enriched in the Deepwater Horizon deep-sea oil plume. Isme J. 6 (2), 451–460.

McClain, C., Rex, M., Etter, R., 2009. Patterns in deep-sea macroecology. In: Witman, J.D., Roy, K. (Eds.), Marine Macroecology. The University of Chicago Press, Chicago, USA, pp. 440.

McIntyre, A.D. (Ed.), 2010. Life in the world's oceans: diversity, distribution and abundance. Wiley-Blackwell, Oxford, UK.

Montagna, P., Harper, J.D.E., 1996. Benthic infaunal long-term response to offshore production platforms in the Gulf of Mexico. Can. J. Fish Aquat. Sci. 53 (11), 2567–2588.

Morse, J.W., Beazley, M.J., 2008. Organic matter in deepwater sediments of the Northern Gulf of Mexico and its relationship to the distribution of benthic organisms. Deep-Sea Res. II 55 (24–26), 2563–2571.

Narayanaswamy, B.E., Bett, B.J., 2011. Macrobenthic biomass relations in the Faroe-Shetland channel: An Arctic-Atlantic boundary environment. PLoS One 6 (4), e18602.

Oey, L.-Y., Lee, H.-C., 2002. Deep eddy energy and topographic rossby waves in the Gulf of Mexico. J. Phys. Oceanogr. 32 (12), 3499–3527.

Pace, M.L., Knauer, G.A., Karl, D.M., Martin, J.H., 1987. Primary production, new production and vertical flux in the eastern Pacific Ocean. Nature 325 (6107), 803–804.

Pavithran, S., Ingole, B., Nanajkar, M., Goltekar, R., 2009. Importance of sieve size in deep-sea macrobenthic studies. Mar. Biol. Res. 5 (4), 391–398.

Pequegnat, W.E., 1983. The ecological communities of the continental slope and adjacent regimes of the northern Gulf of Mexico. A final report by TerEco Corporation for the US Department of the Interior, Minerals Management Service Gulf of Mexico OCS Office Metairie, LA, p. 379.

Pequegnat, W.E., Gallaway, B.J., Pequegnat, L.H., 1990. Aspects of the ecology of the deep-water fauna of the Gulf of Mexico. Am. Zool. 30 (1), 45–64.

Pitcher, C.R., Lawton, P., Ellis, N., Smith, S.J., Incze, L.S., Wei, C.-L., Greenlaw, M.E., Wolff, N.H., Sameoto, J.A., Snelgrove, P.V.R., 2012. Exploring the role of environmental variables in shaping patterns of seabed biodiversity composition in regional-scale ecosystems. J. Appl. Ecol. 49 (3), 670–679.

Plaza-Reséndiz, I.P., 2006. Variación de la estructura comunitaria béntica de la planicie abisal del Golfo de México, Universidad Nacional Autónoma de México (UNAM), D.F. México.

R Development Core Team, 2011. R: A language and environment for statistical computing, Vienna, Austria. R Foundation for Statistical Computing.

Rex, M.A., Etter, R.J., Morris, J.S., Crouse, J., McClain, C.R., Johnson, N.A., Stuart, C.T., Deming, J.W., Thies, R., Avery, R., 2006. Global bathymetric patterns of standing stock and body size in the deep-sea benthos. Mar Ecol Prog Ser 317, 1–8.

Richardson, G.E., Nixon, L.D., Bohannon, C.M., Kazanis, E.G., Montgomery, T.M., Gravois, M.P., 2008. Deepwater Gulf of Mexico 2008: America's fffshore energy future. U.S. Department of the Interior, Minerals Management Service, Gulf of Mexico OCS Region, New Orleans, LA, p. 112.

Richardson, M.D., Young, D.K., 1987. Abyssal benthos of the Venezuela Basin, Caribbean Sea: standing stock considerations. Deep-Sea Res. I 34 (2), 145–164.

Ross, C.B., Gardner, W.D., Richardson, M.J., Asper, V.L., 2009. Currents and sediment transport in the Mississippi Canyon and effects of Hurricane Georges. Cont. Shelf Res. 29 (11–12), 1384–1396.

Rowe, G.T., 1971. Benthic biomass in the Pisco, Peru upwelling. Investigacion Pesquera 35 (1), 127–135.

Rowe, G.T., 1983. Biomass and production of deep-sea macrobenthos. In: Rowe, G.T. (Ed.), Deep-sea Biol. Wily-interscience, New York, pp. 97–121.

Rowe, G.T., Deming, J.W., 2011. An alternative view of the role of heterotrophic microbes in the cycling of organic matter in deep-sea sediments. Mar. Biol. Res. 7 (7), 629–636.

Rowe, G.T., Kennicutt, M.C., 2008. Introduction to the Deep Gulf of Mexico Benthos program. Deep-Sea Res. II 55 (24–26), 2536–2540.

Rowe, G.T., Kennicutt, M.C., 2009. Northern Gulf of Mexico continental slope habitats and benthic ecology study, final report. U.S. Dept. of the Interior, Minerals Management Service, Gulf of Mexico OCS Region Regional Office, New Orleans, LA., p. 417.

Rowe, G.T., Lohse, A., Hubbard, F., Boland, G.S., Escobar Briones, E., Deming, J., 2003. Preliminary trophodynamic carbon budget for the Sigsbee Deep benthos, Northern Gulf of Mexico. Am. Fish. Soc. Sym. 36, 225–238.

Rowe, G.T., Menzel, D., 1971. Quantitative benthic samples from the deep Gulf of Mexico with some comments on the measurement of deep-sea biomass. Bull. Mar. Sci. 21, 556–566.

Rowe, G.T., Morse, J., Nunnally, C., Boland, G.S., 2008a. Sediment community oxygen consumption in the deep Gulf of Mexico. Deep-Sea Res. II 55 (24–26), 2686–2691.

Rowe, G.T., Polloni, P.T., Horner, S.G., 1974. Benthic biomass estimates from the northwestern atlantic ocean and the northern Gulf of Mexico. Deep-Sea Res. Oceanogr. Abstracts 21 (8), 641–650.

Rowe, G.T., Wei, C.-L., Nunnally, C., Haedrich, R., Montagna, P., Baguley, J.G., Bernhard, J.M., Wicksten, M., Ammons, A., Briones, E.E., Soliman, Y., Deming, J.W., 2008b. Comparative biomass structure and estimated carbon flow in food webs in the deep Gulf of Mexico. Deep-Sea Res. II 55 (24–26), 2699–2711.

Ruhl, H.A., Ellena, J.A., Smith, K.L., 2008. Connections between climate, food limitation, and carbon cycling in abyssal sediment communities. Proc. Nat. Acad. Sci. 105 (44), 17006–17011.

Santschi, P.H., Rowe, G.T., 2008. Radiocarbon-derived sedimentation rates in the Gulf of Mexico. Deep-Sea Res. II 55 (24–26), 2572–2576.

Sarkar, D., 2008. Lattice: multivariate data visualization with R. Springer, New York.

Sibuet, M., Olu, K., 1998. Biogeography, biodiversity and fluid dependence of deep-sea cold-seep communities at active and passive margins. Deep-Sea Res. II 45 (1–3), 517–567.

Smith, C.R., Berelson, W., Demaster, D.J., Dobbs, F.C., Hammond, D., Hoover, D.J., Pope, R.H., Stephens, M., 1997. Latitudinal variations in benthic processes in the abyssal equatorial Pacific: control by biogenic particle flux. Deep-Sea Res. II 44 (9–10), 2295–2317.

Smith, K.L., Ruhl, H.A., Bett, B.J., Billett, D.S.M., Lampitt, R.S., Kaufmann, R.S., 2009. Climate, carbon cycling, and deep-ocean ecosystems. Proc. Nat. Acad. Sci. 106 (46), 19211–19218.

Smith, S.J., Ellis, N., Pitcher, C.R., 2011. Conditional variable importance in R package extendedForest. R vignette. 〈http://gradientforest.r-forge.r-project.org/Conditional-importance.pdf〉.

Snelgrove, P., 2010. Discoveries of the Census of Marine Life: Making ocean life count. Cambridge University Press, Cambridge, UK.

Soliman, Y., Wicksten, M., 2007. *Ampelisca mississippiana*: A new species (Crustacea: Amphipoda: Gammaridea) from the Mississippi Canyon (Northern Gulf of Mexico). Zootaxa 1389, 45–54.

Soliman, Y.S., Wade, T.L., 2008. Estimates of PAHs burdens in a population of ampeliscid amphipods at the head of the Mississippi Canyon (N. Gulf of Mexico). Deep-Sea Res. II 55 (24–26), 2577–2584.

Strobl, C., Boulesteix, A.-L., Kneib, T., Augustin, T., Zeileis, A., 2008. Conditional variable importance for random forests. BMC Bioinformatics 9 (1), 307.

Suess, E., 1980. Particulate organic carbon flux in the oceans-surface productivity and oxygen utilization. Nature 288 (5788), 260–263.

Sweetman, A., Witte, U., 2008. Response of an abyssal macrofaunal community to a phytodetrital pulse. Mar. Ecol. Prog. Ser. 355, 73–84.
Thiel, H., 1975. The size structure of the deep-sea benthos. Internationale Revue der gesamten Hydrobiologie und Hydrographie 60, 575–606.
Valentine, D.L., Kessler, J.D., Redmond, M.C., Mendes, S.D., Heintz, M.B., Farwell, C., Hu, L., Kinnaman, F.S., Yvon-Lewis, S., Du, M., Chan, E.W., Tigreros, F.G., Villanueva, C.J., 2010. Propane respiration jump-starts microbial response to a deep oil spill. Science 330 (6001), 208–211.
Vetter, E.W., Dayton, P.K., 1998. Macrofaunal communities within and adjacent to a detritus-rich submarine canyon system. Deep-Sea Res. II 45 (1-3), 25–54.
Wade, T.L., Soliman, Y., Sweet, S.T., Wolff, G.A., Presley, B.J., 2008. Trace elements and polycyclic aromatic hydrocarbons (PAHs) concentrations in deep Gulf of Mexico sediments. Deep-Sea Res. II 55 (24–26), 2585–2593.
Wei, C.-L., Rowe, G., Hubbard, G., Scheltema, A., Wilson, G., Petrescu, I., Foster, J., Wicksten, M., Chen, M., Davenport, R., Soliman, Y., Wang, Y., 2010a. Bathymetric zonation of deep-sea macrofauna in relation to export of surface phytoplankton production. Mar. Ecol. Prog. Ser. 399, 1–14.
Wei, C.-L., Rowe, G.T., Escobar-Briones, E., Boetius, A., Soltwedel, T., Caley, M.J., Soliman, Y., Huettmann, F., Qu, F., Yu, Z., Pitcher, C.R., Haedrich, R.L., Wicksten, M.K., Rex, M.A., Baguley, J.G., Sharma, J., Danovaro, R., MacDonald, I.R., Nunnally, C.C., Deming, J.W., Montagna, P., Lévesque, M., Weslawski, J.M., Wlodarska-Kowalczuk, M., Ingole, B.S., Bett, B.J., Billett, D.S.M., Yool, A., Bluhm, B.A., Iken, K., Narayanaswamy, B.E., 2010b. Global patterns and predictions of seafloor biomass using Random Forests. PLoS One 5 (12), e15323.
Wei, C.-L., Rowe, G.T., Nunnally, C., Wicksten, M.K., 2012. Anthropogenic "litter" and macrophyte detritus in the deep northern Gulf of Mexico. Mar. Pollut. Bull.
Wiseman, W.J., Sturges, W., 1999. Physical oceanography of the Gulf of Mexico: Processes that regulate its biology. In: Kumpf, H., Steidinger, K., Sherman, K. (Eds.), The Gulf of Mexico large marine ecosystem: Assessment, sustainability and management. Blackwell Science, Malden, MA, pp. 77–92.
Witte, U., Wenzhofer, F., Sommer, S., Boetius, A., Heinz, P., Aberle, N., Sand, M., Cremer, A., Abraham, W.R., Jorgensen, B.B., Pfannkuche, O., 2003. In situ experimental evidence of the fate of a phytodetritus pulse at the abyssal sea floor. Nature 424 (6950), 763–766.
Yool, A., Shepherd, J.G., Bryden, H.L., Oschlies, A., 2009. Low efficiency of nutrient translocation for enhancing oceanic uptake of carbon dioxide. J. Geophys. Res. 114 (C8), C08009.
Zar, J., 1984. Biostatistical Analysis. Prentice Hall, New Jersey.